Self-consistent signal-to-noise analysis of the statistical behavior of analog neural networks and enhancement of the storage capacity

Masatoshi Shiino
Department of Applied Physics, Tokyo Institute of Technology, 2-12-1, Ohokayama, Meguro-ku, Tokyo, 152, Japan

Tomoki Fukai
Department of Electronics, Tokai University, 1117, Kitakaname, Hiratsuka-shi, Kanagawa, 259-12, Japan
(Received 7 December 1992)

Based on the self-consistent signal-to-noise analysis (SCSNA) capable of dealing with analog neural networks with a wide class of transfer functions, enhancement of the storage capacity of associative memory and the related statistical properties of neural networks are studied for random memory patterns. Two types of transfer functions with the threshold parameter θ are considered, which are derived from the sigmoidal one to represent the output of three-state neurons. Neural networks having a monotonically increasing transfer function F^{M}, $F^{\mathrm{M}}(u)=\mathrm{sgn}u$ ($|u|>\theta$), $F^{\mathrm{M}}(u)=0$ ($|u|\leq\theta$), are shown to make it impossible for the spin-glass state to coexist with retrieval states in a certain parameter region of θ and α (loading rate of memory patterns), implying the reduction of the number of spurious states. The behavior of the storage capacity with changing θ is qualitatively the same as that of the Ising spin neural networks with varying temperature. On the other hand, the nonmonotonic transfer function F^{NM}, $F^{\mathrm{NM}}(u)=\mathrm{sgn}u$ ($|u|<\theta$), $F^{\mathrm{NM}}(u)=0$ ($|u|\geq\theta$) gives rise to remarkable features in several respects. First, it yields a large enhancement of the storage capacity compared with the Amit-Gutfreund-Sompolinsky (AGS) value: with decreasing θ from $\theta=\infty$, the storage capacity α_c of such a network is increased from the AGS value (≈ 0.14) to attain its maximum value of ≈ 0.42 at $\theta\cong 0.7$ and afterwards is decreased to vanish at $\theta=0$. Whereas for $\theta\gtrsim 1$ the storage capacity α_c coincides with the value $\bar{\alpha}_c$ determined by the SCSNA as the upper bound of α ensuring the existence of retrieval solutions, for $\theta\lesssim 1$ the α_c is shown to differ from the $\bar{\alpha}_c$ with the result that the retrieval solutions claimed by the SCSNA are unstable for $\alpha_c<\alpha<\bar{\alpha}_c$. Second, in the case of $\theta<1$ the network can exhibit a new type of phase which appears as a result of a phase transition with respect to the non-Gaussian distribution of the local fields of neurons: the standard type of retrieval state with $r\neq 0$ (i.e., finite width of the local field distribution), which is implied by the order-parameter equations of the SCSNA, disappears at a certain critical loading rate α_0, and for $\alpha\leq\alpha_0$ a qualitatively different type of retrieval state comes into existence in which the width of the local field distribution vanishes (i.e., $r=0^+$). As a consequence, memory retrieval without errors becomes possible even in the saturation limit $\alpha\neq 0$. Results of the computer simulations on the statistical properties of the novel phase with $\alpha\leq\alpha_0$ are shown to be in satisfactory agreement with the theoretical results. The effect of introducing self-couplings on the storage capacity is also analyzed for the two types of networks. It is conspicuous for the networks with F^{NM}, where the self-couplings increase the stability of the retrieval solutions of the SCSNA with small values of θ, leading to a remarkable enhancement of the storage capacity.

PACS number(s): 05.90.+m, 87.10.+e, 05.70.Fh, 02.50.−r

I. INTRODUCTION

The theory of neural networks with symmetric connections as content addressable memory has enjoyed much progress for the past decade [1–5]. Statistical mechanics of spin glasses has contributed a lot to obtaining the knowledge of equilibrium properties of the symmetric networks associated with memory recall dynamics [6], particularly in the case of recurrent-type networks of formal neurons subject to stochastic updating [3–5,7]. Among the quantities characterizing network performances are the storage capacity and the number of spurious states. The storage capacity of the stochastic networks or the Boltzmann machine is given as the limit of the loading rate for the existence of the ergodic component called the retrieval state in the language of thermodynamic phase transitions [7].

Analog neural networks [1(b),2] with deterministic updating, in which output of each neuron taking on continuous values is described by a transfer function, seemed difficult to deal with using a statistical mechanical approach based on the spin-glass theory. Evaluating precisely the storage capacity of the analog neural networks was a key issue together with understanding how the performances of analog neural networks compare with those of the Boltzmann machine, although it was considered that no qualitative differences between the two types of networks should be expected, as long as sigmoidal-type transfer functions are used.

Recently those problems were solved by the authors [8–10] and other researchers [11–13] as well, and an advantage of using analog neural networks for associative memory was discussed extensively in terms of the storage capacity [8,11] and the density of spurious states of the

networks [9,10,12]. In particular, it was found that the analog neural networks with the transfer function $F(u)=\tanh\beta u$ are closely related with the stochastic neural networks of Ising spin type, as is expected, and that the difference between the two can just be attributed to the matter of the so-called Onsager reaction field term [14] which appears in the Thouless-Anderson-Palmer (TAP) equation for the Ising spin neural networks [15]. In other words, the naive TAP equation without that term, by definition, for the analog neural networks, in turn, results in the appearance of an output proportional term [8,16] in the local field which is involved in the set of equations for the order parameters. It is the output proportional term that makes the distribution of the local field non-Gaussian and leads to an enhancement of the storage capacity of the analog neural networks [8,16].

The structure of the key term characteristic to analog neural networks can be properly understood by following the recently developed systematic method of self-consistent signal-to-noise analysis [16] (hereafter referred to as SCSNA). The SCSNA may be viewed as an extension of probability theoretic signal-to-noise analysis [17–19] to the case of evaluating the storage capacity with small retrieval errors allowed [20,21]. The essence of the method is to properly extract the noise part of the local field experienced by a neuron of the networks in the course of the "renormalization" process. The SCSNA can deal with analog neural networks with a wide class of transfer functions [22] and moreover was shown to be applicable to networks with a certain type of asymmetric connections [16].

It will be of interest to study, by taking advantage of the SCSNA, the problem of how the storage capacity is correlated with or determined by the shape of the transfer function of neurons. In the present paper we investigate the possibility of expecting an enhancement of the storage capacity of deterministic analog neural networks by taking transfer functions corresponding to the output of three-state neurons which can be assumed to take on values -1, 0, and 1. The present work is motivated by an attempt to gain insight into the issue of which part of the transfer function for the typical binary neurons $F(u)=\mathrm{sgn}(u)$ is responsible for the sustaining of retrieval states for associative memory. To this end, it will be convenient to work with two kinds of odd transfer functions describing three-state neurons which are discriminated by the region of membrane potential giving null output, D_0. One is the case in which D_0 contains $u=0$, i.e., $F^{\mathrm{M}}(u)=\mathrm{sgn}u$ $(|u|>\theta)$, $F^{\mathrm{M}}(u)=0$ $(|u|\leq\theta)$ and hence the center-cutoff-type transfer function F^{M} is a monotonically increasing function. The parameter θ should be expected to play the role of temperature for the Ising spin neural networks, with the larger θ giving the smaller storage capacity [23]. We would like to see if there is any other outcome to be seen of getting the output activity of neurons diminished to 0 around $u=0$.

The other type of transfer function we consider is the one for which D_0 extends over up to $u=\infty$, i.e., $F^{\mathrm{NM}}(u)=\mathrm{sgn}u$ $(|u|<\theta)$, $F^{\mathrm{NM}}(u)=0$ $(|u|\geq\theta)$. Our primary concern is with investigating to what extent the cutting off of the output activity of neurons with the input beyond a certain level will affect the network performances. In such an end-cutoff-type transfer function case, it is of particular interest to see what will happen to the networks with $\theta<1$, in view of the fact that in the case of the Hopfield model with $F(u)=\mathrm{sgn}(u)$ for a finite number of random memory patterns $F(1)=1$ is required for the retrieval state to be equilibrium points of the updating dynamics.

Using the SCSNA we have found several interesting features of the memory recall properties of the networks with the above-mentioned two types of transfer functions. In the case of the center-cutoff-type transfer functions, spin-glass states manifest themselves through a first kind of phase transition in the phase diagram of α-θ plane unlike the continuous transition in the commonly known case [7], and hence for small values of α there exist retrieval states which do not make the spin-glass state coexist. The storage capacity α_c, on the other hand, behaves qualitatively the same way when θ is changed as that of the standard analog neural networks having sigmoidal-type transfer functions does with its analog gain changed [8,11].

By contrast, for the networks with the end-cutoff-type transfer functions, a remarkable enhancement of the storage capacity ensues. As θ is decreased from infinity, the storage capacity $\alpha_c(\theta)$ increases, surpassing the Amit-Gutfreund-Sompolinsky (AGS) value of ≈ 0.14 until it attains a maximum value of ≈ 0.42 at $\theta\cong 0.7$, and decreases to 0 at vanishing θ. While the $\alpha_c(\theta)$ with $\theta\gtrsim 1$ can be determined by the SCSNA as the limit value of α ensuring the existence of fixed-point-type attractors of the order-parameter equations representing retrieval states, the storage capacity for $\theta\lesssim 1$ is given as the value of α yielding the onset of instability of the SCSNA-retrieval state. Due to the nonmonotonic transfer function, the existence of a Liapunov function, in general, is no longer expected. In fact, the onset of instability for small θ is related to the appearance of oscillatory behavior of the networks, which is confirmed by numerical simulations.

Of particular interest is the occurrence of a kind of phase transition at a certain loading rate $\alpha_0(\theta)$ when $\theta<1$, with respect to the width of the non-Gaussian distribution of the local fields of neurons. The transition arises from the vanishing at α_0 of the standard type of solutions to the order-parameter equations of the SCSNA such that with α approaching α_0 from above, r tends to zero and the standard type of solution with $r\neq 0$ for the retrieval states no longer exists for $\alpha\leq\alpha_0$, where $\sqrt{r}$ is proportional to the width of the local field distribution. When $\alpha\leq\alpha_0$, noise part in the local field vanishes and $r=0^+$ holds. As a consequence, below the transition point a perfect memory recall with the "tolerance" overlap $g=1$ can be ensured. The occurrence of such a phase transition is closely related not only to the existence of an output proportional term characteristic to analog neural networks in the local field, but also to the shape of an "effective" transfer function or renormalized output claimed by the SCSNA in such that it is likely, in general, to require discontinuous jumps as a decreasing function of noise z in the local field.

From the viewpoint of the enhancement of the storage capacity, it is also of interest to investigate the effect of the self-couplings, which are expected to be useful for that purpose if the magnitude of those is appropriately limited so as not to increase the number of spurious states. To our knowledge, a systematic analysis of the role played by the self-couplings in associative memory retrieval including a quantitative evaluation of the storage capacity seems lacking. Whereas the effect of the self-couplings on the enhancement of the storage capacity is not remarkable in the case of the center-cutoff-type transfer functions, it proves quite large in the networks with the end-cutoff-type transfer functions. In the latter case, the self-couplings lead to an increase of the stability of the retrieval solutions claimed by the SCSNA which without the self-couplings exhibit instability. As a consequence, the networks with a certain amount of self-couplings enjoy a remarkable enhancement of the storage capacity. If the problem of the appearance of spurious states can be put aside, in the case of $\epsilon=1$ (ϵ: magnitude of the self-couplings) the network exhibits a maximum storage capacity of $\alpha_c \cong 0.78$ which is attained at $\theta \cong 0.27$. The ϵ dependence of the storage capacity, however, is not monotonic with increasing ϵ, but yields an optimal ϵ to maximize the storage capacity for each θ.

Except that the storage capacity in the case of small θ and ϵ is determined from the onset of oscillatory instability, the results of the SCSNA showing the large enhancement of the storage capacity and the occurrence of the phase transition at $\alpha=\alpha_0$ are in excellent agreement with the results obtained from the numerical simulations conducted on the networks of $100 \leq N \leq 700$ with the end-cutoff-type transfer functions.

The outline of the present paper is as follows. We present in Sec. II an explanation of the SCSNA used in the later sections to make the paper self-contained. Although the substantial body of the method together with its application was already reported elsewhere, we will elaborate on elucidating how the SCSNA is self-consistent in treating signal and noise parts in the local field and how it differs from other similar methods. The present description can be viewed as a reformulated version of the original SCSNA. Section III is devoted to the analysis of neural networks with the center-cutoff-type transfer functions. In Sec. IV the evaluation of the storage capacity for the case of the end-cutoff-type transfer functions is presented. A remarkable enhancement of the storage capacity and the occurrence of a new type of phase transition are exhaustively described. Theoretical results are compared with the results of numerical simulations. Finally in Sec. V we present a brief summary and discussions. Appendix A is devoted to showing how the SCSNA is available for the case of the Amit-Gutfreund-Sompolinsky theory. Appendix B is intended to give a systematic derivation of the equations which are shown in Sec. IV to describe the retrieval phase with $\epsilon=1$ for $\alpha \leq \alpha_0$.

II. SELF-CONSISTENT SIGNAL-TO-NOISE ANALYSIS

A. Analog neural networks

We begin by presenting model neural networks of analog neurons with a transfer function F which represents input-output relation of neurons. The analog network dynamics [1(b)] takes the form of

$$\frac{d}{dt}u_i=-u_i+\sum_{j=1}^{N}J_{ij}F(u_j)+I, \quad i=1,\ldots,N , \tag{2.1a}$$

where u's represent membrane potentials, I an external current, and N the number of total neurons. Equation (2.1a) is closely related to another type of equation describing the outputs of analog neurons of the networks, which should read

$$\frac{d}{dt}v_i=-v_i+F\left[\sum_{j=1}^{N}J_{ij}v_j+I\right], \quad i=1,\ldots,N . \tag{2.1b}$$

In fact, when one sets

$$u_i=\sum_{j=1}^{N}J_{ij}v_j+I ,$$

(2.1a) turns out to follow form (2.1b), under the condition that I be constant in time. In particular, in the case where matrix J_{ij} is invertible, the two sets of equations are equivalent to each other.

The synaptic connections J_{ij} are assumed to be symmetric and given by the Hebb rule

$$J_{ij}=\frac{1}{N}\sum_{\mu=1}^{p}(\xi_i^{(\mu)}-a)(\xi_j^{(\mu)}-a)[1+(\epsilon-1)\delta_{ij}] . \tag{2.2}$$

Here, $\{\xi_i^{(\mu)}\}$ ($\mu=1,\ldots,p$, $i=1,\ldots,N$) denote p ($=\alpha N$) sets of biased random patterns for memories which are specified by independent identical distribution with mean a:

$$P_r(\xi_i^{(\mu)})=\frac{1+a}{2}\delta(\xi_i^{(\mu)}-1)+\frac{1-a}{2}\delta(\xi_i^{(\mu)}+1) . \tag{2.3}$$

We incorporated into the synaptic connections the self-coupling whose strength is measured by ϵ to observe its effect on the storage capacity. The case of no self-couplings is implied by $\epsilon=0$, and $\epsilon=1$ corresponds to the case of a formal extension of the local Hebb rule for J_{ii}. Since too strong self-couplings may lead to a significant increase of the number of spurious states, we will confine ourselves only to the case of weak self-couplings.

Equilibrium states of the network are given by $(d/dt)u_i=0$ [$(d/dt)v_i=0$] for $i=1,\ldots,N$, in (2.1a) [(2.1b)]. Denoting output $F(u_i)$ at equilibrium by x_i [$=v_i(t=\infty)$], we define the local field of ith neuron at equilibrium by

$$h_i=\sum_{j=1}^{N}J_{ij}x_j+I , \tag{2.4}$$

which equals $u_i(t=\infty)$. Then a set of equations determining equilibrium states of the network reads

$$x_i=F(h_i), \quad i=1,\ldots,N . \tag{2.5}$$

Defining the order-parameter overlaps

$$m^{(\mu)}=\frac{1}{N}\sum_{j}(\xi_j^{(\mu)}-a)x_j, \quad \mu=1,\ldots,p , \tag{2.6}$$

we consider retrieval solutions to Eq. (2.5) in which

$$m^{(1)}=O(1), \quad m^{(\mu)}=O(1/\sqrt{N}) \quad \text{for } \mu \geq 2 . \tag{2.7}$$

The so-called retrieval states will be given by the retrieval solutions which are stable.

B. Systematic treatment of the local field

The SCSNA starts with rewriting the local field (2.4) in terms of the overlaps as

$$h_i=(\xi_i^{(1)}-a)m^{(1)}+\sum_{\nu\geq 2}(\xi_i^{(\nu)}-a)m^{(\nu)}+I +\alpha(1-a^2)(\epsilon-1)x_i . \tag{2.8}$$

The sum over $\nu \geq 2$ in (2.8), which we call the "residual part," is usually taken to be a random variable with "mean" $\alpha(1-a^2)x_i$ in the conventional approach [10,20], owing to the simple observation that the average of each $(\xi_i^{(\nu)}-a)(\xi_j^{(\nu)}-a)x_j$ $(i\neq j)$ over the random patterns should be expected to vanish. [The naive noise $\sum_{\nu\geq 2}(\xi_i^{(\nu)}-a)m^{(\nu)}-\alpha(1-a^2)x_i$ then has its mean 0.] This observation, however, does not hold true. One has to be careful to deal with the correlation between $(\xi_i^{(\nu)}-a)$ and $m^{(\nu)}$ for each $\nu \geq 2$. The SCSNA properly deals with the correlation to extract a systematic part from the naive noise.

In our first report of the SCSNA [16], we described the essential part of the method in rather a heuristic manner. Here, we will present a reformulated scheme of the SCSNA detailing the self-consistency of the method. We first assume that the residual part splits into "pure" noise part $z_{i,\mu}$ and a systematic part given as the term proportional to the output, γx_i, in such that for any $\mu \geq 2$

$$\sum_{\nu\neq\mu,1}(\xi_i^{(\nu)}-a)m^{(\nu)}=\overline{z_{i,\mu}}+\gamma x_i , \tag{2.9}$$

and hence that

$$h_i=(\xi_i^{(1)}-a)m^{(1)}+(\xi_i^{(\mu)}-a)m^{(\mu)}+I +\overline{z_{i,\mu}}+\gamma x_i+\alpha(1-a^2)(\epsilon-1)x_i . \tag{2.10}$$

Here, we reserved the term of $O(1/\sqrt{N})$, $(\xi_i^{(\mu)}-a)m^{(\mu)}$, for the sake of analysis below. Then it can well be assumed that $z_{i,\mu}$ is independent of $(\xi_i^{(\mu)}-a)$. The spirit of the SCSNA is in the self-consistent determination of the splitting of the residual part into $z_{i,\mu}$ and γx_i.

The output $x_i=F(h_i)$ then must satisfy

$$x_i=F[(\xi_i^{(1)}-a)m^{(1)}+(\xi_i^{(\mu)}-a)m^{(\mu)}+I+\overline{z_{i,\mu}}+\Gamma x_i] , \tag{2.11}$$

with

$$\Gamma=\gamma+\alpha(1-a^2)(\epsilon-1) . \tag{2.12}$$

This will be solved in the form

$$x_i=\tilde{F}[(\xi_i^{(1)}-a)m^{(1)}+(\xi_i^{(\mu)}-a)m^{(\mu)}+I+\overline{z_{i,\mu}}] . \tag{2.13}$$

Substituting this into (2.6) gives

$$m^{(\mu)}=\frac{1}{N}\sum_j(\xi_j^{(\mu)}-a)\{\tilde{F}[(\xi_j^{(1)}-a)m^{(1)}+I+\overline{z_{j,\mu}}]+(\xi_j^{(\mu)}-a)m^{(\mu)}\tilde{F}'[(\xi_j^{(1)}-a)m^{(1)}+I+\overline{z_{j,\mu}}]\}, \quad \mu\geq 2 . \tag{2.14}$$

Here, the right-hand side of (2.13) was expanded up to first order in $(\xi_j^{(\mu)}-a)m^{(\mu)}$, which still contributes $O(1/\sqrt{N})$ to $m^{(\mu)}$ $(\mu \geq 2)$. For the time being, we assume that the function $\tilde{F}$ has its derivative. Then one obtains $m^{(\mu)}$ from (2.13) in the form

$$m^{(\mu)}=\frac{1}{KN}\sum_j(\xi_j^{(\mu)}-a)\tilde{F}[(\xi_j^{(1)}-a)m^{(1)}+I+\overline{z_{j,\mu}}], \quad \mu\geq 2 , \tag{2.15}$$

with

$$K=1-\frac{1}{N}\sum_j(\xi_j^{(\mu)}-a)^2\tilde{F}'[(\xi_j^{(1)}-a)m^{(1)}+I+\overline{z_{j,\mu}}] . \tag{2.16}$$

Utilizing (2.15) and (2.16), one can compute the sum $\sum_{\nu\neq\mu,1}(\xi_i^{(\nu)}-a)m^{(\nu)}$ as

$$\begin{aligned}\sum_{\nu\neq\mu,1}(\xi_i^{(\nu)}-a)m^{(\nu)}&=\sum_j\sum_{\nu\neq\mu,1}\frac{1}{KN}(\xi_i^{(\nu)}-a)(\xi_j^{(\nu)}-a)\tilde{F}[(\xi_j^{(1)}-a)m^{(1)}+I+\overline{z_{j,\nu}}]\\ &=\frac{1}{KN}\sum_{\nu\neq\mu,1}(\xi_i^{(\nu)}-a)^2\tilde{F}[(\xi_i^{(1)}-a)m^{(1)}+I+\overline{z_{i,\nu}}]\\ &\quad+\sum_{j\neq i}\sum_{\nu\neq\mu,1}\frac{1}{KN}(\xi_i^{(\nu)}-a)(\xi_j^{(\nu)}-a)\tilde{F}[(\xi_j^{(1)}-a)m^{(1)}+I+\overline{z_{j,\nu}}] .\end{aligned} \tag{2.17}$$

The first term in the last line of (2.17), which was extracted by setting $j=i$ in the sum over j, turns out to be proportional to the output x_i, because

$$\frac{1}{KN}\sum_{\nu\neq\mu,1}(\xi_i^{(\nu)}-a)^2\tilde{F}[(\xi_i^{(1)}-a)m^{(1)}+I+\overline{z_{i,\nu}}]=\frac{\alpha}{K}\langle(\xi_i^{(\nu)}-a)^2\tilde{F}[(\xi_i^{(1)}-a)m^{(1)}+I+\overline{z_{i,\nu}}]\rangle_{\xi_i^{(\nu)}}$$
$$=\frac{\alpha}{K}\langle(\xi_i^{(\nu)}-a)^2\rangle_{\xi_i^{(\nu)}}\tilde{F}[(\xi_i^{(1)}-a)m^{(1)}+I+\overline{z_{i,\nu}}]$$
$$=\frac{\alpha}{K}(1-a^2)x_i\ . \tag{2.18}$$

Here we used the assumption of independence of $\overline{z_{i,\nu}}$ from $\xi_i^{(\nu)}$ and also noted that the $O(1/\sqrt{N})$ term $(\xi_i^{(\mu)}-a)m^{(\mu)}$ in the expression (2.13) for the output x_i can be neglected in the present situation. We now see that the SCSNA claims

$$\gamma=\frac{\alpha}{K}(1-a^2)\ . \tag{2.19}$$

Since the second term $\sum_{j\neq i}$ in the last line of (2.17) is a sum of almost uncorrelated random variables and its average over the random patterns $\{\xi_i^{(\nu)}\}_{i=1,\ldots,N}$ $(\nu\geq 2)$ vanishes, that term has to give rise to the pure noise $z_{i,\mu}$ as assumed in the scheme of the SCSNA:

$$\overline{z_{i,\mu}}=\sum_{j\neq i}\sum_{\nu\neq\mu,1}\frac{1}{KN}(\xi_i^{(\nu)}-a)(\xi_j^{(\nu)}-a)\tilde{F}[(\xi_j^{(1)}-a)m^{(1)}+I+\overline{z_{j,\nu}}]\ , \tag{2.20}$$

with $\langle\overline{z_{i,\mu}}\rangle=0$. Noting that the cross correlation of each pair of the terms of the $\overline{z_{i,\mu}}$ vanishes owing to the absence of correlation between $z_{i,\mu}$ and $(\xi_i^{(\mu)}-a)$, one also has

$$\langle\bar{z}_{i,\mu}^2\rangle=\frac{1}{K^2N^2}\sum_{\nu\neq\mu,1}\sum_{j\neq i}\langle(\xi_i^{(\nu)}-a)^2\rangle\langle(\xi_j^{(\nu)}-a)^2\rangle\langle\tilde{F}[(\xi_j^{(1)}-a)m^{(1)}+I+\overline{z_{j,\nu}}]^2\rangle$$
$$=\frac{\alpha(1-a^2)^2}{K^2}\sum_j\frac{1}{N}\langle\tilde{F}[(\xi_j^{(1)}-a)m^{(1)}+I+\overline{z_{j,\nu}}]^2\rangle\ , \tag{2.21}$$

where $\langle\ \rangle$ denotes average over the random patterns $\{\xi_i^{(\nu)}\}_{i=1,\ldots,N}$ $(\nu\geq 2)$. We noted from (2.20) that $\overline{z_{i,\mu}}$ should be independent of μ in the limit $N\to\infty$. Then subscript μ of $z_{i,\mu}$ could be dropped at this stage of the analysis. It is also reasonable to expect from (2.20) and (2.21) that the statistical property of $\overline{z_i}$ is i independent and obeys an identical Gaussian distribution. For the SCSNA to work, it is necessary to assume the self-averaging property to hold so that the site average can be replaced by an average over the random patterns and random variable $\bar{z}$:

$$\frac{1}{N}\sum_j\cdots\to\langle\cdots\rangle_{\{\xi^\nu\}_{\nu=1,\ldots,p},\bar{z}}\quad(N\to\infty)\ , \tag{2.22}$$

in which the random variation of $\overline{z_i}$ from site to site can be described by single noise $\bar{z}$ obeying an identical Gaussian distribution. Accordingly, it follows from (21) that variance σ^2 of noise $\bar{z}$ is determined self-consistently by

$$\sigma^2\equiv\langle\bar{z}^2\rangle_{\bar{z}}=\frac{\alpha(1-a^2)^2}{K^2}\langle\langle\tilde{F}[(\xi^{(1)}-a)m^{(1)}+I+\bar{z}]^2\rangle\rangle_{\xi^{(1)},\bar{z}}\ , \tag{2.23}$$

where $\langle\langle\ \rangle\rangle_{\xi^{(1)},\bar{z}}$ denotes the average over the condensed pattern $\xi^{(1)}$ and random variable $\bar{z}$ with the probability density $D(\bar{z})=(1/\sqrt{2\pi}\sigma)\exp(-\bar{z}^2/2\sigma^2)$.

In the same way, (2.16) for K can be rewritten as

$$K=1-(1-a^2)\langle\langle\tilde{F}'[(\xi^{(1)}-a)m^{(1)}+I+\bar{z}]\rangle\rangle_{\xi^{(1)},\bar{z}}\ , \tag{2.24}$$

and for the relevant overlap $m^{(1)}$

$$m^{(1)}=\langle\langle(\xi^{(1)}-a)\tilde{F}[(\xi^{(1)}-a)m^{(1)}+I+\bar{z}]\rangle\rangle_{\xi^{(1)},\bar{z}}\ . \tag{2.25}$$

In writing (2.25) we omitted the $O(1/\sqrt{N})$ term $(\xi_i^{(\mu)}-a)m^{(\mu)}$ in (2.13) which has just a vanishing contribution in the limit $N\to\infty$.

Substituting (2.19) into (2.10), one has an implicit expression for the renormalized local field in which the site i dependence of (2.10) is absorbed into the distributions of random variables $\xi^{(1)}$ and $\bar{z}$;

$$h(\xi^{(1)},\bar{z})=(\xi^{(1)}-a)m^{(1)}+I+\bar{z}+\Gamma Y(\xi^{(1)},\bar{z})\ , \tag{2.26}$$

$$\Gamma=\alpha\left[\frac{1}{K}+\epsilon-1\right](1-a^2)\ , \tag{2.27}$$

with the renormalized output $Y(\xi^{(1)},\bar{z})\equiv F(h(\xi^{(1)},\bar{z}))$ being self-consistently determined by [16]

$$Y(\xi^{(1)},\bar{z})=F[(\xi^{(1)}-a)m^{(1)}+I+\bar{z}+\Gamma Y(\xi^{(1)},\bar{z})]\ . \tag{2.28}$$

Note that $\tilde{F}[(\xi^{(1)}-a)m^{(1)}+I+\bar{z}]$ in Eqs. (2.23)–(2.25) is

nothing but the $Y(\xi^{(1)},\bar{z})$.

We can see from (2.12) or (2.27) that the output proportional term ΓY in the local field consists of the self-coupling related term $\alpha(1-a^2)(\epsilon-1)Y$ and the squeezed output γY due to the renormalization of the residual part of the local field (2.9). Note that even when the "bare" self-couplings are absent, $\epsilon=0$, "effective" self-couplings arise to yield the output proportional term ΓY as the sum of the two terms. Here, the term "renormalization" is used in two ways. First, it means expressing a distribution of a physical quantity over sites (neurons) in terms of a function of random variables, in this case $\xi^{(1)}$ and $\bar{z}$ obeying a Gaussian distribution. Second, our "renormalization" procedure reminds us of the renormalization scheme used in the many-body theory in the sense that it extracts the output proportional term of γY due to "effective" self-couplings from the residual part of the local field.

We would like to comment on the terminology for the SCSNA. When the retrieval state for the condensed pattern $\xi^{(1)}$ ensures nearly perfect recall [for example, $m^{(1)}\approx 1$ in the case of $a=0$ and $F(u)=\tanh\beta u$ with $\beta\gg 1$], output $Y(\xi^{(1)},\bar{z})$ can be considered approximately to represent the signal, $Y(\xi^{(1)},\bar{z})=\xi^{(1)}$. Then the squeezing of the output by means of the systematic renormalization procedure we have employed will correspond to the self-consistent discriminating of signal from noise. For this reason, the SCSNA will deserve being referred to as such.

Finally with the change of variables

$$q=\frac{K^2\sigma^2}{(1-a^2)^2\alpha}\ ,$$
$$\sqrt{\alpha r}=\sigma\ ,$$
$$U=\frac{1-K}{1-a^2}\ , \tag{2.29}$$
$$\frac{\bar{z}}{\sigma}=z\ ,$$

Eqs. (2.23)–(2.25) are transformed to a more familiar form of equations [16],

$$m=\left\langle \int_{-\infty}^{\infty} dz \frac{\exp(-z^2/2)}{\sqrt{2\pi}}(\xi-a)Y(\xi,z)\right\rangle\ , \tag{2.30a}$$

$$q=\left\langle \int_{-\infty}^{\infty} dz \frac{\exp(-z^2/2)}{\sqrt{2\pi}}Y(\xi,z)^2\right\rangle\ , \tag{2.30b}$$

$$U\sqrt{\alpha r}=\left\langle \int_{-\infty}^{\infty} dz \frac{\exp(-z^2/2)}{\sqrt{2\pi}}zY(\xi,z)\right\rangle\ , \tag{2.30c}$$

with

$$Y(\xi,z)=F[(\xi-a)m+I+\sqrt{\alpha r}z+\Gamma Y(\xi,z)]\ , \tag{2.30d}$$

$$\Gamma=\alpha(1-a^2)\left[\frac{1}{1-U(1-a^2)}+\epsilon-1\right]\ , \tag{2.30e}$$

$$q=\frac{\{1-(1-a^2)U\}^2 r}{(1-a^2)^2}\ , \tag{2.30f}$$

where $\langle\ \rangle$ denotes the average over ξ. Equation (2.30) constitutes a set of equations describing the retrieval states which yield $m^{(1)}\neq 0$. Although we have so far assumed differentiability of $\tilde{F}$ in deriving the above equations, the assumption may be lifted in practice, when we note that (2.30) do not involve the derivative of Y any longer.

C. The ΓY term and properties of analog neural networks

We note first that the set of equations is exactly the same as the one obtained by applying the replica symmetric theory to analog neural networks [8,11]. This will imply that the assumption of the self-averaging property, which is the crux of the SCSNA, should be justified as long as the neural networks are free from undergoing the replica-symmetry breaking instability transition [15] at which an ultrametric structure begins to appear and the self-averaging property will no longer be expected. As was seen above, the SCSNA, which requires no more than quite easy and transparent calculations to yield (2.29), turns out to be particularly suitable to get microscopic but relevant information of how the local field distribution $P(h)$ is determined in connection with the appearance of the ΓY. The situation should be contrasted with the case of using the replica symmetric theory for analog neural networks, where the calculations involved are cumbersome and the origin of the ΓY term is hidden behind the mathematical trick of the saddle point method [8]. We may say that the mechanism for the appearance of the ΓY term was clarified thanks to the SCSNA.

As we pointed out in the previous paper [16], the presence of the output proportional term ΓY in the local field is characteristic of the deterministic analog neural networks, in which the TAP equation (2.1a) is, by definition, free of the so-called Onsager reaction field which is required in the case of the stochastic Ising spin neural networks [15]. In other words, when one deals with the TAP equation [10] of the stochastic Ising spin neural networks, the output proportional term ΓY must be canceled out by the reaction field term to yield the well-known result of the AGS theory, in which an equation of the form (2.30d) with $\Gamma=0$ and $F(\cdots)=\tanh\beta(\cdots)$ follows. One can easily see this by a straightforward application of the SCSNA to such a TAP equation. We give a brief description of the derivation of the AGS result [7] based on the SCSNA in Appendix A.

Let us proceed to consider the effects of the ΓY term on the properties of the analog neural networks as well as on the analysis itself. All of the effects will be related to the fact that (2.30d), which only implicitly gives the output, has to be solved properly before performing the integrations over z.

1. Maxwell rule for determining the available solution $Y(\xi,z)$

Equation (2.30d) for $Y(\xi,z)$ in general admits more than one solution. In that case a kind of Maxwell rule should be applied to choose the appropriate solution [8,16,22]. This is suggested from the replica symmetric theory applied to analog neural networks [8] in which the available solution Y is the one that maximizes the ex-

ponent of the integrand appearing in the saddle point method. We give a brief explanation of the convenient recipe by taking, as an example for which the replica symmetric theory is also available, a typical sigmoid-type transfer function $F(u)=\tanh\beta u$ with $I=0$ and $a=0$.

Suppose (2.30d) is solved graphically as shown in Fig. 1, where any of the solutions Y is given as an intersection point of the straight line $H=\Gamma Y+\xi m+\sqrt{\alpha r}z$ with the curve $H=F^{-1}(Y)$. In the case where three intersection points are allowed to exist for a certain value of Γ, the outer one with the larger enclosed area is to be selected. The middle point has to be discarded since it should give an unstable solution. The solution Y corresponding to that outer point would make the Y-related exponent function arising in the saddle point method larger than the outer point at the opposite side would, if one worked with replica symmetric theory. When z takes on the value $z=-\xi m/\sqrt{\alpha r}$ and an equal area is ensured in the two enclosed areas, both the outer intersection points can equally maximize the exponent, yielding two solutions for $Y(z)$. Accordingly, the solution $Y(z)$ turns out to exhibit a jump at $z=-\xi m/\sqrt{\alpha r}$.

2. *Enhancement of storage capacity*

Such a jump makes the renormalized output $Y(z)$ get considerably increased around $z=-\xi m/\sqrt{\alpha r}$ compared with the original transfer function F with $\Gamma=0$, i.e., $F(\xi m+\sqrt{\alpha r}z)$, as is shown in Fig. 2. Even when (2.30d) yields a unique solution for $Y(z)$ and the jump does not appear, a *positive* Γ turns out to result in an increase of the analog gain of a *monotonically increasing* transfer function such as the one of sigmoidal type. The effectively increased analog gain is expected to lead to an increase in the storage capacity. In fact, the storage capacity of the analog neural networks with the transfer function $F(u)=\tanh\beta u$ [8] was shown to be larger than the corresponding Ising spin networks for which $\Gamma=0$. In this connection, an introduction of the self-couplings into the synaptic interactions ($\epsilon>0$) is, in general, considered to give rise to an enhancement of the storage capacity, since it increases the Γ. Quantitatively evaluating the change with ϵ of the storage capacity will be of interest. In the following sections we will treat this problem.

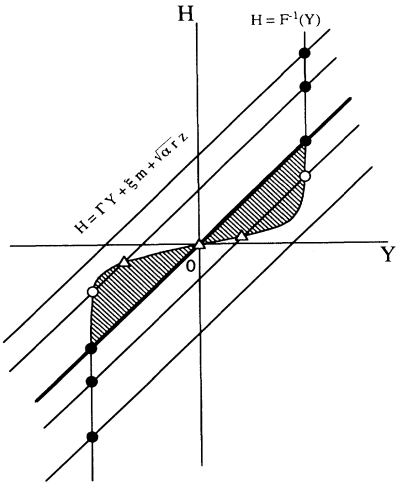

FIG. 1. Application of the Maxwell rule and a graphical representation of $F^{-1}(Y)=\Gamma Y+\xi m+\sqrt{\alpha r}z$ for solving Y as a function of z. The two relevant solutions can coexist for the equation in which $H=\Gamma Y+\xi m+\sqrt{\alpha r}z$ is specified by the thick straight line (i.e., $z=-\xi m/\sqrt{\alpha r}$) ensuring the equal-area condition in the Maxwell rule. The filled circles, circles, and triangles represent relevant solutions (points), which are the most stable, less stable ones, and unstable ones, respectively.

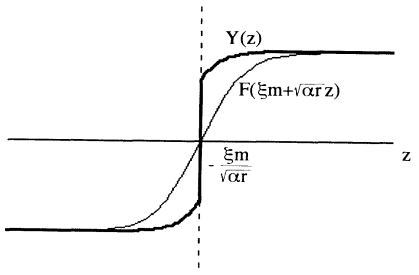

FIG. 2. Schematic comparison between $Y(z)$ and $F(\xi m+\sqrt{\alpha r}z)$. The presence of the ΓY term in the local field is seen to result in an effective increase in analog gain of the transfer function, leading to an enhancement of the storage capacity.

It should be noted that when one uses nonmonotonic neurons as will be treated in Sec. IV, a case of $\Gamma<0$ can occur due to a negative U in the absence of the self-couplings. In spite of the negativeness of Γ, the storage capacity will be shown to be remarkably enhanced. In that case a major ingredient for the enhancement of the storage capacity is the shape of the nonmonotonic transfer function rather than the term ΓY itself. However, making the Γ positive by an introduction of the self-couplings ($\epsilon>0$) turns out to result in a further increase of the storage capacity, as long as ϵ is not very large.

Another effect of the ΓY term in the local field worth noting is on the distribution of the local field itself. The distribution of the local field in the case of the stochastic Ising spin neural networks is, according to the AGS theory, Gaussian except for the replica-symmetry breaking region, because the replica symmetric solution of the AGS theory claims $\Gamma=0$. When $\Gamma\neq0$ as in the present case of analog neural networks, the renormalized local field $h(\xi,z)=\Gamma Y+\xi m+\sqrt{\alpha r}z$ is determined through the renormalized output $Y(\xi,z)$, which is subject to the nonlinear transformation (2.30d) in z. As a consequence, the $h(\xi,z)$ is nonlinear in z, and a non-Gaussian distribution of the local field $h(\xi,z)$ follows. We will see later that a non-Gaussian distribution of the local field manifests itself in a pronounced manner in the case of transfer functions with certain discontinuous jumps.

III. NETWORKS OF THREE-STATE NEURONS WITH THE CENTER-CUTOFF-TYPE TRANSFER FUNCTIONS

When one is concerned with the relationship between the shape of a transfer function describing input-output

relation of analog neurons and the properties of analog networks as associative memory, it will be of importance to investigate the behavior of networks with variants of the transfer function of the formal neuron taking binary outputs. We would like to explore the effect of cutting off the output activity of the formal neurons on the storage capacity and on the related properties of the attractor neural networks. One may then ask to what extent the output of binary neurons can be cut off under the condition that the memory retrieval is still ensured, or whether the cutting of the output activity leads to any improvement of network performances such as the reduction of the number of spurious states and the enhancement of the storage capacity. Among the manners of cutting off the output of binary neurons which attract our attention are two types of treatments, both of which formally constitute three-state neurons. The first one gives the center-cutoff-type transfer function which is obtained by cutting off the output corresponding to the membrane potential near the threshold. The second type defines the end-cutoff-type transfer functions in which right and left wings of the output activity of the binary neurons are cut off.

A. Application of the SCSNA

The transfer functions with which we are concerned in the present section are those of the center-cutoff-type. They are given by

$$F^{\mathrm{M}}(u)=\begin{cases}\mathrm{sgn}u, & |u|>\theta \\ 0, & |u|\le\theta\end{cases}, \tag{3.1}$$

and shown in Fig. 3. Here, θ is a parameter measuring a degree of the deviation from the transfer function of two-state neurons $F(u)=\mathrm{sgn}u$. In what follows, assuming nonbiased random patterns with $a=0$ in (2.2), we consider the equilibrium properties of updating dynamics (2.1). We first note that when $a=0$ and the transfer function F is odd in the variable, i.e., $F(u)=-F(-u)$, as in the present case, the average over ξ in the set of equations (2.30) can easily be performed and the resultant set of equations takes the same form, except that $\langle\ \rangle$ is omitted with ξ being replaced by 1: $m=\int_{-\infty}^{\infty}dz\ Y(1,z)(1/\sqrt{2\pi})\exp(-z^2/2)$ and so on.

When applying the SCSNA in Sec. II, we have to solve

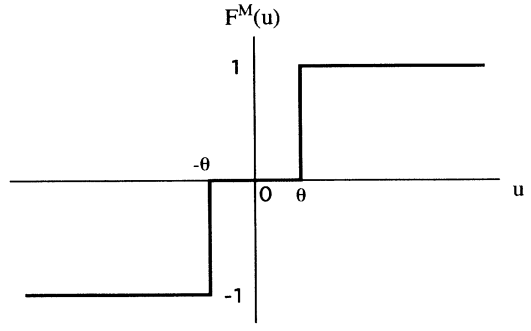

FIG. 3. Center-cutoff-type transfer function $F^{\mathrm{M}}(u)$ with a parameter θ.

(2.30d) to obtain the renormalized output $Y(z)$, which is necessary for the Gaussian integrations involved. We take into account the Maxwell rule mentioned earlier to solve

$$F^{-1}(Y)=m+\Gamma Y+\sqrt{\alpha r}z\ , \tag{3.2}$$

which is equivalent to (2.30d) with $a=0$, $\xi=1$, and

$$\Gamma=\alpha\left[\frac{1}{1-U}+\epsilon-1\right]. \tag{3.3}$$

Here, the inverse function F^{-1} is formally defined as what is obtained by a symmetric transformation of the curve $y=F(x)$ with respect to the line $y=x$. Two cases should occur according to the value of Γ; case I, $\Gamma\ge 2\theta$ and case II, $0<\Gamma<2\theta$, as is shown in Figs. 4(a) and 4(b), respectively.

Case I: $\Gamma\ge 2\theta$. Using the Maxwell rule to select the

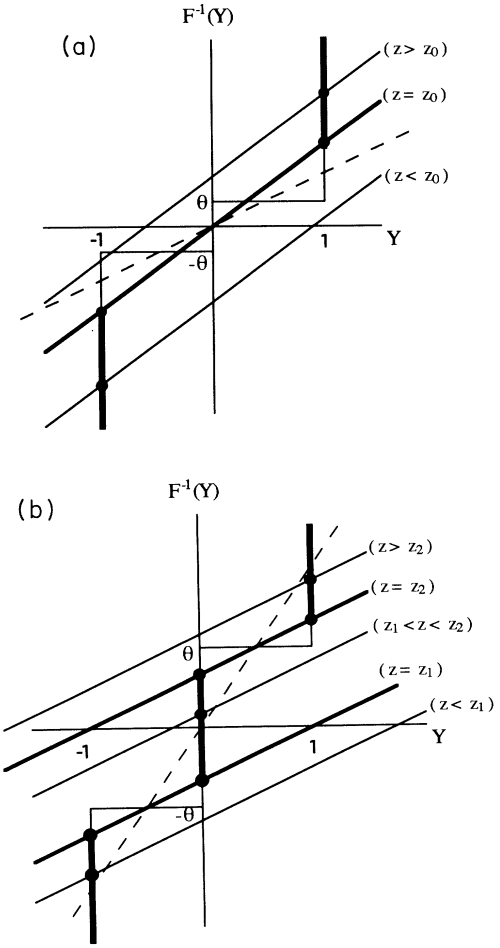

FIG. 4. A graphical representation of $F^{-1}(Y)=m+\Gamma Y+\sqrt{\alpha r}z$ for obtaining Y as a function of z with the aid of the Maxwell rule, when $F=F^{\mathrm{M}}$: (a) $\Gamma\ge 2\theta$, (b) $0<\Gamma<2\theta$. Two relevant solutions are allowed to coexist for the equation specified by the slant thick lines with $z=z_0$ (a) and $z=z_1$, $z=z_2$ (b). The filled circles represent the available solutions. The dashed line with $\Gamma=2\theta$ is shown only for reference.

available solution from the five solutions (intersection points) at values of z near z_0, one immediately obtains the renormalized output $Y(z)$:

$$Y(z)=\begin{cases}1, & z>z_0\\ -1, & z<z_0\end{cases}, \tag{3.4}$$

with

$$z_0=\frac{-m}{\sqrt{\alpha r}} .$$

We see that the renormalized output $Y(z)$ simply coincides with a binary output irrespective of the values of θ, as long as $\Gamma\geq 2\theta$. Then the problem is just reduced to that of the transfer function with $\theta=0$, which corresponds to the case of the zero-temperature Ising spin neural network of the AGS theory [7].

In fact, substituting the $Y(z)$ into (2.30) yields $q=1$ and

$$m=-2N[0,z_0] , \tag{3.5a}$$

$$\sqrt{\alpha r}=\sqrt{\alpha}+\frac{2}{\sqrt{2\pi}}e^{-z_0^2/2} , \tag{3.5b}$$

where $N[X,Y]$ denotes a Gaussian integral:

$$N[X,Y]=\int_X^Y dz\frac{1}{\sqrt{2\pi}}e^{-z^2/2} . \tag{3.6}$$

From (3.5) the storage capacity $\alpha_c=0.138$ follows.

Case II: $0<\Gamma<2\theta$. Applications of the Maxwell rule yield the renormalized output $Y(z)$ with jumps at $z=z_1$ and $z=z_2$:

$$Y(z)=\begin{cases}1, & z>z_2\\ 0, & z_1<z<z_2\\ -1, & z<z_1\end{cases}, \tag{3.7}$$

with

$$z_1=\frac{-\theta-m+\Gamma/2}{\sqrt{\alpha r}} ,$$

$$z_2=\frac{\theta-m-\Gamma/2}{\sqrt{\alpha r}} .$$

The $Y(z)$ is seen to take a similar form to the original F of the three-state neurons. Substituting the $Y(z)$ into (2.30), one obtains a set of equations for m, r, and U:

$$m=-N[0,z_1]-N[0,z_2] , \tag{3.8a}$$

$$(1-U)^2 r=1-N[0,z_2]+N[0,z_1] , \tag{3.8b}$$

$$U\sqrt{\alpha r}=\frac{1}{\sqrt{2\pi}}(e^{-z_2^2/2}+e^{-z_1^2/2}) . \tag{3.8c}$$

Retrieval states and spin-glass ones of the networks are characterized, respectively, by $m\neq 0$, $q\neq 0$, and $m=0$, $q\neq 0$. They are determined by numerically solving (3.5) or (3.8) for m, r, and U. The value of Γ is not known *a priori* but determined in the course of solving those equations. The storage capacity will be given, as usual, by the upper bound of the loading rate for the existence of the retrieval states.

B. Results

1. *Case of no self-couplings* ($\epsilon=0$)

We first deal with the case of no self-couplings ($\epsilon=0$). We display in Fig. 5 the phase diagram drawn on the α-θ plane showing the θ dependence of the storage capacity and the phase boundary of the spin-glass state as well. The parameter θ, which represents a kind of threshold of a three-state neuron and hence the degree of the deviation from the simple binary output, apparently differs from the analog gain β of a sigmoidal-type transfer function. However, so far as the behavior of the α_c with changing θ is concerned, it is seen to be qualitatively the same as that of the analog networks with changing β; the α_c decreases from its maximum of $\alpha_c=0.138$, as θ increases from $\theta=0$ to 1 at which α_c vanishes [23].

Characteristic to the present transfer function with the parameter θ is the manner of the onset of the spin-glass states. In a common type of analog networks with analog gain β, the spin-glass state ($m=0$, $q\neq 0$) emerges at a certain critical value β_{SG} through a continuous phase transition from the paramagnetic state ($m=0$, $q=0$), as β is increased with α kept fixed. This is because such a transition occurs as a result of the so-called tangent bifurcation for which the linear stability analysis with respect to an infinitesimally small q makes sense and a change in the β is relevant for the stability change. By contrast, for the transfer functions (2.1) there occurs no such continuous transition, since the slope at the origin ($u=0$) of the transfer functions remains zero. In other words, the paramagnetic state $m=0$, $q=0$ will be stable irrespective of the value of θ. In fact, the phase boundary for the spin-glass state in Fig. 5 is given as a discontinuous transition line on which the spin-glass state abruptly appears (disappears). Figure 6 depicts an example of the variation

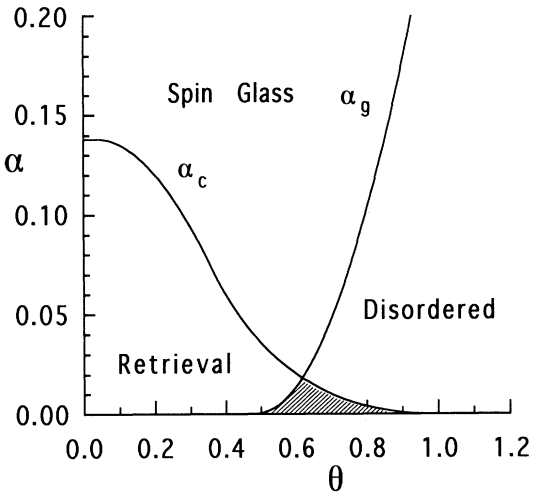

FIG. 5. Phase diagram ($\epsilon=0$) representing the θ dependence of the storage capacity and the phase boundary of the spin-glass phase. The retrieval states are allowed in the region below the α_c curve and the spin-glass ones in the whole region on the left side of the α_g curve. A characteristic feature is the appearance of a region in the retrieval phase outside the spin-glass one.

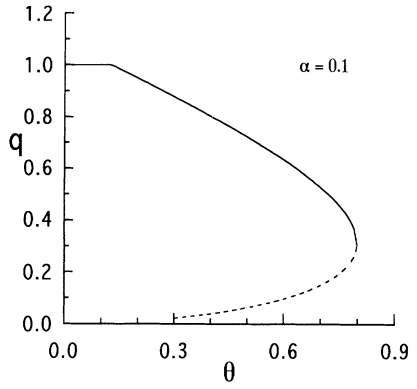

FIG. 6. Plot of spin-glass order parameter q against θ when $\alpha=0.1$. The network is seen to undergo a phase transition of a first kind between the disordered (paramagnetic) phase and the spin-glass one.

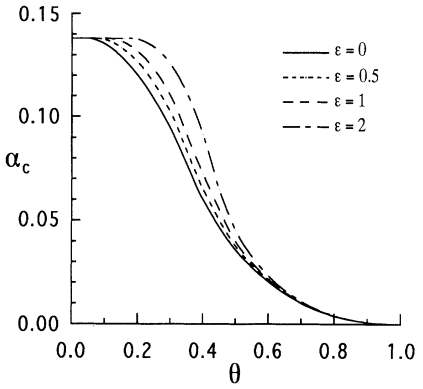

FIG. 7. Plot of α_c against θ for several values of ϵ.

of the spin-glass order parameter q with the change of θ for a fixed value of α. We see that the spin-glass state abruptly disappears at a certain value of θ, when θ is increased from 0. A remarkable feature seen in the phase diagram Fig. 5 is the appearance of the region (shaded), though small, of retrieval states in which the spin-glass state is not allowed to coexist. Since the spin-glass states give rise to spurious states which are obstacles for associative memory recall, the appearance of such a region in the phase diagram will be promising to improve the network performances in terms of reducing the number of spurious states.

2. *Effect of the self-couplings* ($\epsilon > 0$)

From the expression (3.3) for Γ, it follows that an increase of ϵ, the strength of the self-couplings, leads to an increase of Γ. Recall the effect of Γ mentioned in the preceding section on the storage capacity for associative memory of the analog networks. We now can observe clearly, from (3.7), the role played by Γ in defining effective transfer functions based on the "bare" transfer functions F (3.1). The threshold value θ of the bare transfer function is effectively transformed into $\theta_{\text{eff}}=\theta-\Gamma/2$ for the effective transfer function which could yield the renormalized output (3.7). Then (3.3) tells us that the effect of introducing the self-couplings with magnitude ϵ is to decrease the value of θ by $\alpha\epsilon/2$. In view of the above-mentioned result that the storage capacity α_c is a decreasing function of θ, such an effective decrease ($\epsilon>0$) of the θ due to the presence of the self-couplings has to increase α_c, leading to the enhancement of the storage capacity, compared with the case of no self-couplings. We display in Fig. 7 the ϵ dependence of the α_c vs θ curve, which confirms the above argument. It can be seen, however, that the maximum value of $\alpha_c=0.138$ is not exceeded by any increase of the strength of the self-couplings. It is noted that for a fixed value of ϵ the storage capacity α_c remains constant with $\alpha_c=0.138$, unless θ exceeds a certain value $\theta_0(\epsilon)$. This phenomenon, which is more pronounced as ϵ is increased, is a result of the occurrence of the case 1 with $\Gamma\geq 2\theta$, which is just attributed to the presence of the output proportional term ΓY in the local field. Since the introduction of the self-couplings gives rise to only a little enhancement of the storage capacity while increasing the number of spurious states to deteriorate the network performances, overall effect of the self-couplings may not be so promising in the case of the present transfer functions. This situation should be contrasted with the other case which we will deal with in the next section.

IV. END-CUTOFF-TYPE TRANSFER FUNCTIONS AND STATISTICAL PROPERTIES OF THE NETWORKS OF NONMONOTONIC NEURONS

In the present section, we study the neural networks of three-state neurons derived as a result of another treatment of cutting of the output activity of two-state neurons. To be specific, we consider the networks having end-cutoff-type transfer functions which are defined by

$$F^{\text{NM}}(u)=\begin{cases}\text{sgn}u, & |u|<\theta\\ 0, & |u|\geq\theta\end{cases}, \tag{4.1}$$

and displayed in Fig. 8. θ is a parameter controlling the cutting of activity of a neuron. The transfer function then becomes a nonmonotonic function. As in the preceding section, the synaptic connections are assumed to be given by (2.2) with $a=0$ and the updating rule by (2.1).

A. Case of a finite number of patterns

To observe how the network with a nonmonotonic transfer function works as content addressable memory,

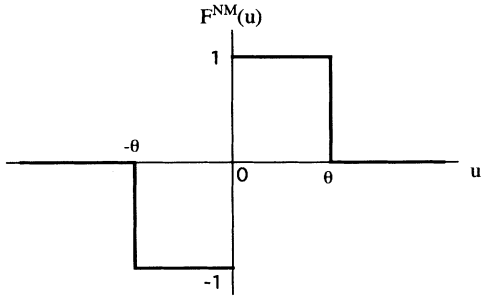

FIG. 8. End-cutoff-type transfer function $F^{\text{NM}}(u)$ with a parameter θ.

we first consider the case in which the number of stored patterns p is finite. Using (2.1b) for the updating rule together with (2.6) for the order-parameter overlaps $\{m^{(\nu)}\}_{\nu=1,\ldots,p}$, the network dynamics turns out to take the simple form

$$\frac{d}{dt}v_i=-v_i+F\left[\sum_{\mu=1}^{p}\xi_i^{(\mu)}m^{(\mu)}\right],\quad i=1,\ldots,N\ . \tag{4.2}$$

Multiplying both hands of (4.2) by $\xi_i^{(\nu)}/N$ ($\nu=1,\ldots,p$) and summing over i, one obtains the set of p-dimensional dynamical equations for the overlaps:

$$\frac{d}{dt}m^{(\nu)}=-m^{(\nu)}+\sum_{\xi}r(\xi)\xi^{(\nu)}F\left[\sum_{\mu=1}^{p}\xi^{(\mu)}m^{(\mu)}\right],$$
$$\nu=1,\ldots,p\ . \tag{4.3}$$

Here, in carrying out the sum over i, we used the concept of sublattice assuming N to be sufficiently large [5,24–30]; a p-dimensional vector $\xi=(\xi^{(1)},\ldots,\xi^{(p)})$ of the hypercube $H^p=\{-1,1\}^p$ represents the sublattice $\{i|\xi_i^{(\nu)}=\xi^{(\nu)},\ \nu=1,\ldots,p\}$ and $r(\xi)$ is the ratio of the size of sublattice ξ to the total number of neurons N. Since the patterns are assumed to be random, $r(\xi)=2^{-p}$ for each ξ.

Assuming $\{m^{(\nu)}\}$ to be close to one of the retrieval states for which $m^{(1)}\neq 0$, $m^{(\nu)}=0$, $2\leq\nu\leq p$, one has

$$\frac{d}{dt}m^{(1)}=-m^{(1)}+F(m^{(1)})\ . \tag{4.4}$$

Then an equilibrium value $m^{(1)}$ is formally determined by

$$m^{(1)}=F(m^{(1)})\ . \tag{4.5}$$

When $F=F^{\mathrm{NM}}$ with $\theta\geq 1$, (4.5) yields the common type of retrieval solutions $m^{(1)}=\pm 1$. On the other hand, for the transfer function F (4.1) with $\theta<1$ which exhibits discontinuous jumps in $|u|<1$, this equation should be interpreted as follows.

We consider the transfer function (4.1) to be given as the limit δ_0, $\delta\to 0+$ of a transfer function $F_{\delta_0\delta}(u)$ with small positive parameters δ_0 and δ representing the degree of the smoothing of the jumps [Fig. 9(a)]. Then (4.5) with $F(u)=F_{\delta_0\delta}(u)$ solves as the intersection point of the two curves representing both hands of (4.5), as is shown in Fig. 9(b). In the limit $\delta\to 0+$, it turns out that

$$m^{(1)}=\pm\theta\ . \tag{4.6}$$

In case one deals with (4.4) with the $\delta=0$ transfer function from the outset, that is, without taking the limit $\delta\to 0+$, the differential equation (4.4) will lose its meaning as soon as the $m^{(1)}$ reaches $m^{(1)}=\pm\theta$. The $m^{(1)}$ thereafter sticks to that value, so to speak. If one is allowed to modify the interpretation of (4.4) by means of a certain treatment like a finite difference scheme as an approximation to a differential equation so as to make such a sticking solution be a meaningful one representing stationarity, (4.6) would be viewed as an equilibrium solution of (4.4).

So far as the theoretical analysis using the SCSNA is concerned in what follows, we will consider that the transfer function (4.1) is given as the limit δ_0, $\delta\to 0+$ of certain continuous functions $F_{\delta_0\delta}(u)$ which are piecewise differentiable.

B. Enhancement of the storage capacity and phase-transition phenomena

We now deal with the networks with extensively many patterns, $p=\alpha N$ ($N\to\infty$). In applying the SCSNA, we have to consider four cases according to the value of Γ; case I, $\Gamma\leq -2\theta$; case II, $-2\theta<\Gamma\leq 0$; case III, $0<\Gamma<\theta$; and case IV, $\Gamma\geq\theta$. Since $a=0$ is assumed and the transfer functions (4.1) are odd, the set of equations (2.30) can be handled by specifying $Y(1,z)$ [$\equiv Y(z)$] alone as in the preceding section.

Case I: $\Gamma\leq -2\theta$. Noting the Maxwell rule [Fig. 10(a)], we solve (2.30d) to obtain the renormalized output $Y(z)$:

$$Y(z)=\begin{cases}0, & z<z_1,\ z_2<z\\ \dfrac{-m-\sqrt{\alpha r}z}{\Gamma}, & z_1<z<z_2\ ,\end{cases} \tag{4.7a}$$

with

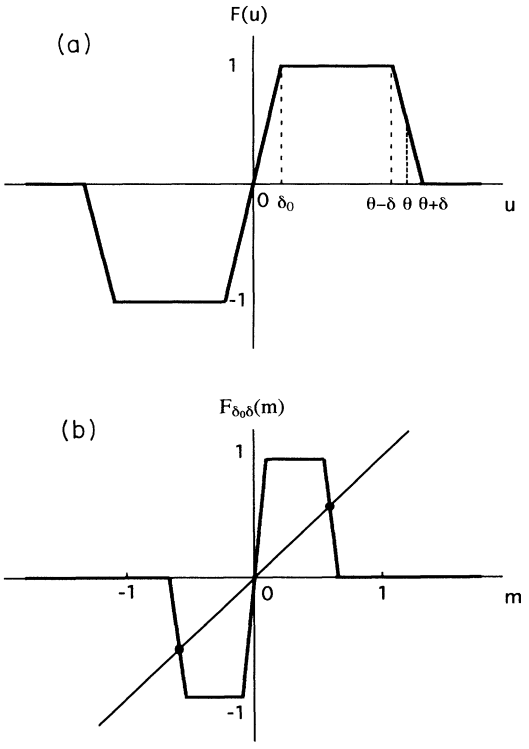

FIG. 9. (a) Transfer function $F_{\delta_0\delta}(u)$ with smoothing parameters δ_0 and δ which approximate $F^{\mathrm{NM}}(u)$. The latter should be defined as the limit δ_0, $\delta\to 0$ of $F_{\delta_0\delta}(u)$ in the context of the SCSNA. (b) The solutions m ($m\neq 0$) to $m=F_{\delta_0\delta}(m)$ can be determined from the intersections of the two curves. In the limit $\delta\to 0$, the m's are seen to approach $\pm\theta$.

$$z_1=\frac{-\theta+\Gamma s-m}{\sqrt{\alpha r}}\ ,$$
$$z_2=\frac{\theta-\Gamma s-m}{\sqrt{\alpha r}}\ , \tag{4.7b}$$

where

$$s=\frac{\theta-\sqrt{-2\Gamma\theta}}{\Gamma}\ . \tag{4.7c}$$

Figure 10(b) displays the profile of the renormalized output $Y(z)$. Substituting the $Y(z)$ into (2.30) yields a set of equations for m, r, and U:

$$m=-\frac{m}{\Gamma}N[z_1,z_2]+\frac{\sqrt{\alpha r}}{\Gamma\sqrt{2\pi}}(e^{-z_2^2/2}-e^{-z_1^2/2})\ , \tag{4.8a}$$

$$(1-U)^2 r=\frac{\alpha r+m^2}{\Gamma^2}N[z_1,z_2]-\frac{2m\sqrt{\alpha r}}{\Gamma^2\sqrt{2\pi}}(e^{-z_2^2/2}-e^{-z_1^2/2})+\frac{\alpha r}{\Gamma^2\sqrt{2\pi}}(z_1e^{-z_1^2/2}-z_2e^{-z_2^2/2})\ , \tag{4.8b}$$

$$U\sqrt{\alpha r}=-\frac{\sqrt{\alpha r}}{\Gamma}N[z_1,z_2]+\frac{m+\sqrt{\alpha r}z_2}{\sqrt{2\pi}\Gamma}e^{-z_2^2/2}-\frac{m+\sqrt{\alpha r}z_1}{\sqrt{2\pi}\Gamma}e^{-z_1^2/2}\ . \tag{4.8c}$$

Case II: $-2\theta<\Gamma\le 0$. Equation (2.30d) together with the Maxwell rule [Fig. 11(a)] yields the renormalized output $Y(z)$:

$$Y(z)=\begin{cases}0, & z<z_1,\quad z_4<z\\ -1, & z_1<z<z_2\\ \dfrac{-m-\sqrt{\alpha r}z}{\Gamma}, & z_2<z<z_3\\ 1, & z_3<z<z_4\ ,\end{cases} \tag{4.9a}$$

with

$$z_1=\frac{-\theta+\Gamma/2-m}{\sqrt{\alpha r}}\ ,$$
$$z_2=\frac{\Gamma-m}{\sqrt{\alpha r}}\ ,$$
$$z_3=\frac{-\Gamma-m}{\sqrt{\alpha r}}\ , \tag{4.9b}$$
$$z_4=\frac{\theta-\Gamma/2-m}{\sqrt{\alpha r}}\ .$$

The profile of the renormalized output is shown in Fig. 11(b). Substituting the $Y(z)$ into (2.30), one obtains

$$m=-N[z_1,z_2]+N[z_3,z_4]-\frac{m}{\Gamma}N[z_2,z_3]+\frac{\sqrt{\alpha r}}{\Gamma\sqrt{2\pi}}(e^{-z_3^2/2}-e^{-z_2^2/2})\ , \tag{4.10a}$$

$$(1-U)^2 r=N[z_1,z_2]+N[z_3,z_4]+\frac{\alpha r+m^2}{\Gamma^2}N[z_2,z_3]-\frac{2m\sqrt{\alpha r}}{\Gamma^2\sqrt{2\pi}}(e^{-z_3^2/2}-e^{-z_2^2/2})+\frac{\alpha r}{\Gamma^2\sqrt{2\pi}}(z_2e^{-z_2^2/2}-z_3e^{-z_3^2/2})\ , \tag{4.10b}$$

$$U\sqrt{\alpha r}=-\frac{\sqrt{\alpha r}}{\Gamma}N[z_2,z_3]-\frac{1}{\sqrt{2\pi}}(e^{-z_1^2/2}+e^{-z_4^2/2})\ . \tag{4.10c}$$

Case III: $0<\Gamma<\theta$. The renormalized output $Y(z)$ of

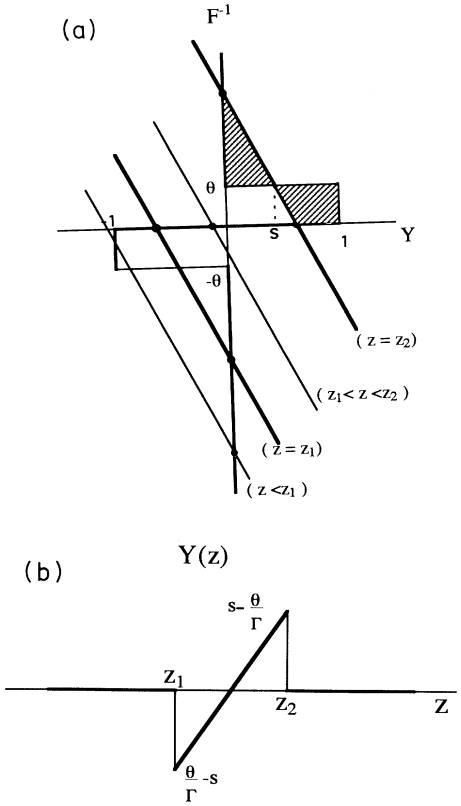

FIG. 10. (a) A graphical representation of $F^{-1}(Y)=m+\Gamma Y+\sqrt{\alpha r}z$ for solving Y as a function of z with use of the Maxwell rule, when $\Gamma\le -2\theta$. Two relevant solutions can coexist for the equation with each case of $z=z_1$ and $z=z_2$ as shown by the thick lines which ensure the equal-area condition in the Maxwell rule. Relevant solutions (points) are marked by filled circles. (b) Profile of the renormalized output $Y(z)$ for $\Gamma\le -2\theta$. The slant line arises from the intersections on the Y axis in (a). The occurrence of the jumps at $z=z_1$ and $z=z_2$ is a direct consequence of the Maxwell rule.

(2.30d) satisfying the Maxwell rule [Fig. 12(a)] is solved as

$$Y(z)=\begin{cases}0, & z<z_1,\ z_4<z \\ \dfrac{-\theta-m-\sqrt{\alpha r}z}{\Gamma}, & z_1<z<z_2 \\ \dfrac{\theta-m-\sqrt{\alpha r}z}{\Gamma}, & z_3<z<z_4 \\ -1, & z_2<z<z_0 \\ 1, & z_0<z<z_3\ , \end{cases} \tag{4.11a}$$

with

$$\begin{aligned} z_0&=\frac{-m}{\sqrt{\alpha r}}\ , \\ z_1&=\frac{-\theta-m}{\sqrt{\alpha r}}\ , \\ z_2&=\frac{-\theta+\Gamma-m}{\sqrt{\alpha r}}\ , \\ z_3&=\frac{\theta-\Gamma-m}{\sqrt{\alpha r}}\ , \\ z_4&=\frac{\theta-m}{\sqrt{\alpha r}}\ . \end{aligned} \tag{4.11b}$$

Figure 12(b) displays its profile. Substitution of (4.11a) into (2.30) gives a set of equations for m, r, and U:

$$m=\frac{-\theta-m}{\Gamma}N[z_1,z_2]-N[z_2,z_0]+N[z_0,z_3]+\frac{\theta-m}{\Gamma}N[z_3,z_4]+\frac{\sqrt{\alpha r}}{\Gamma\sqrt{2\pi}}(e^{-z_2^2/2}+e^{-z_4^2/2}-e^{-z_1^2/2}-e^{-z_3^2/2})\ , \tag{4.12a}$$

$$\begin{aligned}(1-U)^2 r=&N[z_2,z_0]+N[z_0,z_3]+\frac{\alpha r+(\theta+m)^2}{\Gamma^2}N[z_1,z_2]+\frac{\alpha r+(\theta-m)^2}{\Gamma^2}N[z_3,z_4] \\ &+\frac{\alpha r}{\Gamma^2\sqrt{2\pi}}(z_1e^{-z_1^2/2}+z_3e^{-z_3^2/2}-z_2e^{-z_2^2/2}-z_4e^{-z_4^2/2}) \\ &-\frac{2\sqrt{\alpha r}(\theta+m)}{\Gamma^2\sqrt{2\pi}}(e^{-z_2^2/2}-e^{-z_1^2/2})+\frac{2\sqrt{\alpha r}(\theta-m)}{\Gamma^2\sqrt{2\pi}}(e^{-z_4^2/2}-e^{-z_3^2/2})\ , \end{aligned} \tag{4.12b}$$

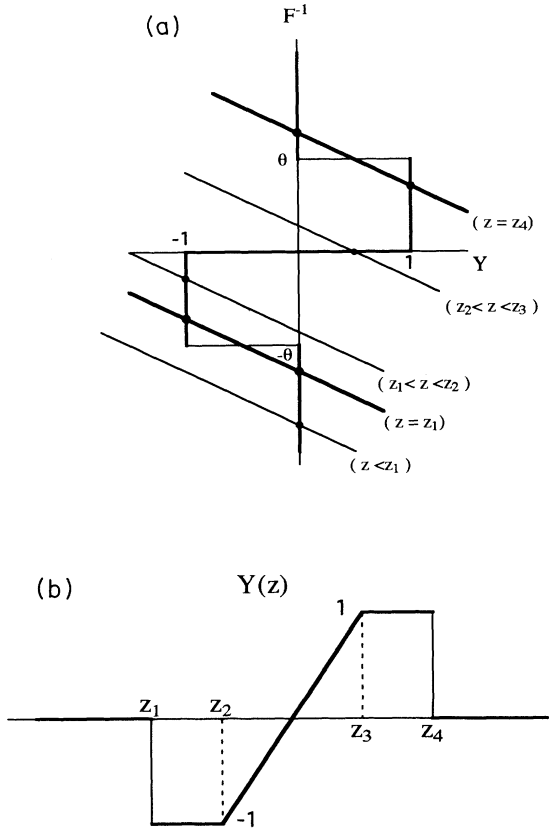

FIG. 11. (a) Same as Fig. 10(a) for $-2\theta<\Gamma\le 0$. (b) Profile of the renormalized output $Y(z)$ for $-2\theta<\Gamma\le 0$.

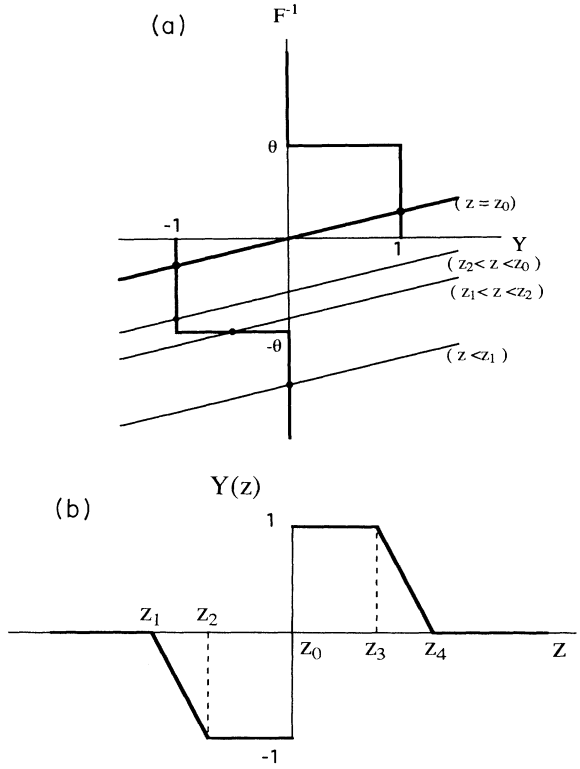

FIG. 12. (a) Same as Fig. 10(a) for $0<\Gamma<\theta$. (b) Profile of the renormalized output $Y(z)$ for $0<\Gamma<\theta$. Note that the jumps at $u=\pm\theta$ exhibited by the original transfer function $F^{\mathrm{NM}}(u)$ have been transformed to the slant lines in the $Y(z)$ due to the presence of the output proportional term ΓY in the local field.

$$U\sqrt{\alpha r} = -\frac{\sqrt{\alpha r}}{\Gamma}(N[z_1,z_2]+N[z_3,z_4])+\frac{2}{\sqrt{2\pi}}e^{-z_0^2/2} . \tag{4.12c}$$

Case IV: $\Gamma \geq \theta$. The renormalized output $Y(z)$ of (2.30d) satisfying the Maxwell rule [Fig. 13(a)] is given by

$$Y(z)=\begin{cases} 0, & z<z_1, \quad z_4<z \\ \dfrac{-\theta-m-\sqrt{\alpha r}z}{\Gamma}, & z_1<z<z_0 \\ \dfrac{\theta-m-\sqrt{\alpha r}z}{\Gamma}, & z_0<z<z_4 , \end{cases} \tag{4.13}$$

where z_0, z_1, and z_4 are given by (4.11b). Figure 13(b) displays its profile.

Substituting the $Y(z)$ into (2.30) gives

$$m=\frac{-\theta-m}{\Gamma}N[z_1,z_0]+\frac{\theta-m}{\Gamma}N[z_0,z_4]+\frac{\sqrt{\alpha r}}{\Gamma\sqrt{2\pi}}(e^{-z_4^2/2}-e^{-z_1^2/2}) , \tag{4.14a}$$

$$(1-U)^2 r=\frac{\alpha r+(\theta+m)^2}{\Gamma^2}N[z_1,z_0]+\frac{\alpha r+(\theta-m)^2}{\Gamma^2}N[z_0,z_4]+\frac{\alpha r}{\Gamma^2\sqrt{2\pi}}(z_1 e^{-z_1^2/2}-z_4 e^{-z_4^2/2})$$
$$-\frac{2\sqrt{\alpha r}(\theta+m)}{\Gamma^2\sqrt{2\pi}}(e^{-z_0^2/2}-e^{-z_1^2/2})+\frac{2\sqrt{\alpha r}(\theta-m)}{\Gamma^2\sqrt{2\pi}}(e^{-z_4^2/2}-e^{-z_0^2/2}) , \tag{4.14b}$$

$$U\sqrt{\alpha r} = -\frac{\sqrt{\alpha r}}{\Gamma}(N[z_1,z_0]+N[z_0,z_4])+\frac{2\theta}{\Gamma\sqrt{2\pi}}e^{-z_0^2/2} . \tag{4.14c}$$

In all the above four cases Γ is given by (3.3). The value of Γ in general is not known *a priori* but determined in the course of solving those equations. It is worth noting that in the case of $\Gamma<0$ (i.e., cases I and II) the sets of equations for m, U, and r presented above hold true even for the transfer function given by F_δ having a finite value of the smoothing parameter δ at $u=|\theta|$, as long as $\delta<|\Gamma|/2$. This immediately follows from the observation that due to the Maxwell rule, such F_δ yields the same renormalized output $Y(z)$ as given in (4.7) or (4.9). It therefore turns out that in the case where the SCSNA yields $\Gamma<0$, there is no need to consider taking the limit $\delta\to 0+$ to avoid the jumps of transfer functions.

The storage capacity will be determined as the limit of the loading rate α for the existence of the retrieval states which are given by the solution $m\neq 0$ of Eq. (4.8), (4.10), (4.12), or (4.14). Our main interest here is twofold in terms of the storage capacity: first in examining the effect of cutting the activity of neurons in the range of membrane potential $|u|>\theta$ as shown in Fig. 8, and second in comparing between such networks with and without the self-couplings. We will deal primarily with the two cases of without ($\epsilon=0$) and with ($\epsilon=1$) self-couplings J_{ii} [Eq. (2.2)], separately.

1. $\epsilon=0$

a. Enhancement of the storage capacity due to non-monotonic neurons. In the absence of the self-couplings

$$\Gamma=\frac{\alpha U}{1-U} . \tag{4.15}$$

Note that if $U<0$, then $\Gamma<0$. Solving numerically (4.8), (4.10), or (4.12) in the case of small ($\theta\lesssim 0.2$), intermediate, or large ($\theta\gtrsim 1.8$) values of θ, respectively, we can obtain the order-parameter overlap m as a function of the loading rate α for a fixed value of θ. Figure 14(a) depicts the variation of m with the change of α for $\theta=1.0$. The $m(\alpha)$ is decreasing with increasing α until it abruptly disappears at the critical value of $\alpha=0.385$, which gives

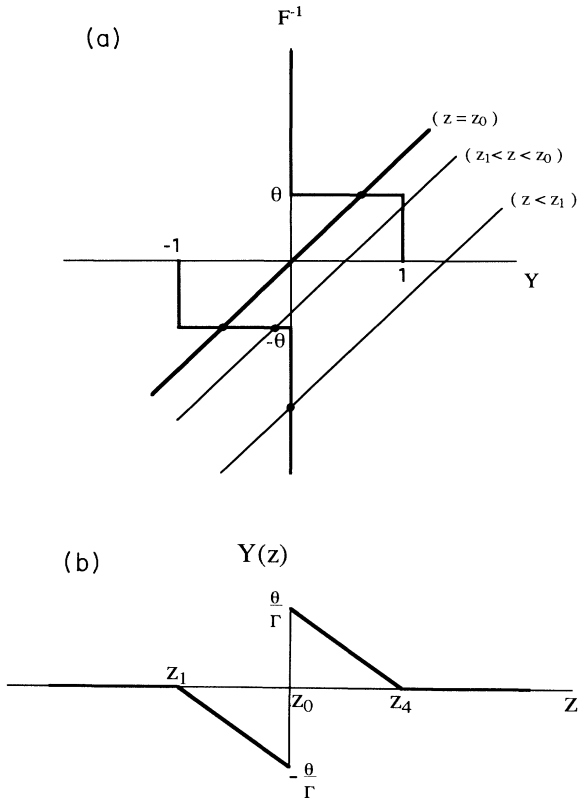

FIG. 13. (a) Same as Fig. 10(a) for $\theta\leq\Gamma$. (b) Profile of the renormalized output $Y(z)$ for $\theta\leq\Gamma$.

the upper bound of α ensuring the existence of the retrieval solutions. Hence we denote such a critical value of α by $\bar{\alpha}_c$. The $\bar{\alpha}_c$ is nothing but the storage capacity, if the retrieval solutions are found to be stable fixed points of (2.1). Since the stability is confirmed numerically in the present case as will be discussed later, it should be surprising for a network with a finite θ to exhibit a larger storage capacity than that of the commonly known Hopfield model ($\alpha_c=0.138$ with $\theta=\infty$).

For the purpose of viewing the extent to which the networks function as associative memory, it will be more convenient to use the tolerance overlap measuring quality of retrieval rather than the order-parameter overlap m which does not account for the activity of neurons with null output.

The tolerance overlap g with respect to the pattern $\{\xi_i\}$ will be defined in terms of the membrane potential u_i or the local field h_i as

$$g=\frac{1}{N}\sum_i \xi_i \mathrm{sgn} u_i$$

$$=\frac{1}{N}\sum_i \xi_i \mathrm{sgn} h_i \ . \tag{4.16}$$

Then, using the renormalized local field $h(\xi,z)$, the g in general can be rewritten as

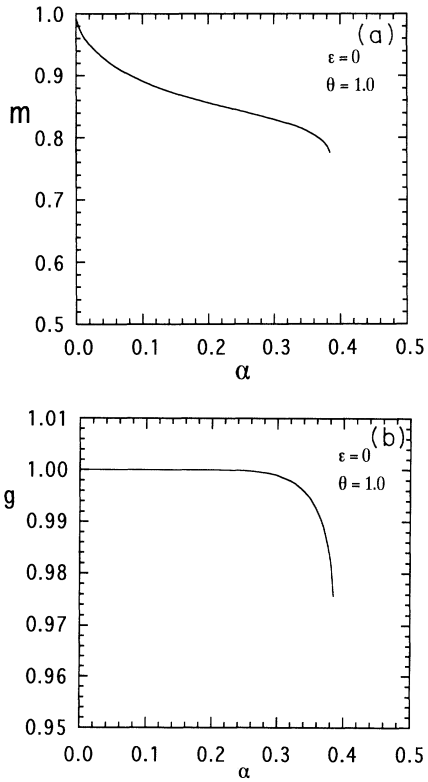

FIG. 14. (a) Plot of the order-parameter overlap m as a function of α for $\theta=1.0(\epsilon=0)$. (b) Plot of the tolerance overlap g as a function of α for $\theta=1.0$ ($\epsilon=0$).

$$g=\left\langle \int_{-\infty}^{\infty} dz \frac{\exp(-z^2/2)}{\sqrt{2\pi}} \xi \,\mathrm{sgn}[h(\xi,z)] \right\rangle \ . \tag{4.17}$$

The renormalized local field $h(\xi,z)=\xi m+\sqrt{\alpha r}z+\Gamma Y$, in the $\epsilon=0$ case, can be easily computed with use of (4.7), (4.9), or (4.11) and we have

$$g=g^{+}\equiv -2N[0,z_0] \ , \tag{4.18}$$

with $z_0=-m/\sqrt{\alpha r}$, or

$$g=g^{-}\equiv N[z_2,-z_3] \quad \text{for case II} \ , \tag{4.19a}$$

$$g=g^{-}\equiv N[z_1,-z_2] \quad \text{for case I} \ , \tag{4.19b}$$

depending on the treatment of sgn0. If sgn0=0 is formally applied to (4.17), $g=g^{-}$ follows in the case of $\Gamma<0$. This, however, yields rather a smaller value, say, $g^{-}=0.971$ for $\theta=1$ and $\alpha=0.38$ compared with g^{+} ($g^{+}=0.983$ for the same θ and α), because $h(\xi,z)=0$ occurs with a finite probability.

On the other hand, when the jump at $u=0$ of the transfer function (4.1) is interpreted as being the limit $\delta_0\to 0+$ of the analog gain $1/\delta_0$, $\mathrm{sgn}[h(\xi,z)]=0$ holds only for $z=-\xi m/\sqrt{\alpha r}$. Then $z>-\xi m/\sqrt{\alpha r}$ implies $\mathrm{sgn}[h(\xi,z)]=1$, which corresponds to the interpretation that $\mathrm{sgn}(0^{+})=1$. In that case one obtains $g=g^{+}$. In accordance with the previously mentioned remark on the treatment of the jumps of the transfer functions, we consider $g=g^{+}$ to be more appropriate for the tolerance overlap of the present system. We display in Fig. 14(b) the plot of $g=g^{+}$ against α for $\theta=1.0$.

The effect of further decreasing θ or further cutting of the output activity of neurons is of considerable interest. As is shown below, the behavior of the networks drastically changes depending on whether $\theta\geq 1$ or $\theta<1$. The networks with $\theta<1$ indeed exhibit a remarkable feature from the viewpoint of the neural network theory of associative memory and statistical mechanical theory of phase transitions.

The m vs α plot obtained from (4.10) for $\theta=0.8$ and 0.4 is displayed in Figs. 15 and 16, respectively (thick curve). Worth mentioning here is that in the case of $\theta<1$ the standard type of retrieval solutions which are given not only by $m\neq 0$ but also by $r\neq 0$ can exist only for a certain interval of α, the upper bound and the lower bound of which are denoted, respectively, by $\bar{\alpha}_c$ and α_0. We show in Fig. 17 the θ dependence of the value of $\bar{\alpha}_c$ together with that of α_0. It should be noted that as θ is decreased from $\theta=\infty$, the $\bar{\alpha}_c$ is seen to increase until it attains a maximum value of as large as ≈ 0.50 at $\theta\cong 0.4$, yielding the possibility of a large enhancement of the storage capacity. As will be studied later by means of numerical simulations, the storage capacity of the networks with $\theta\lesssim 1$, however, is less than $\bar{\alpha}_c$ because of the occurrence of instability, while the storage capacity for $\theta\gtrsim 1$ will turn out to be given by the $\bar{\alpha}_c$.

b. Phase-transition phenomena. We now focus our attention to the problem of what is happening to the network when α approaching the lower bound α_0 at which the standard type of solution to (4.10) disappears as shown in Fig. 15 or 16. Figure 18 depicts the behavior of the solution r of (4.10) for the change of α in the neigh-

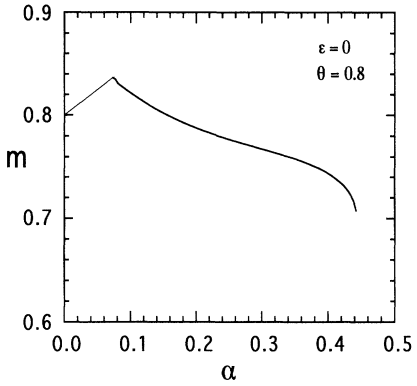

FIG. 15. Plot of m against α for $\theta=0.8$ ($\epsilon=0$). In Figs. 15 and 16 the standard type of retrieval solutions is represented by the thick curve. The thin line denotes m's for the $r=0^+$ phase which occurs as a result of a phase transition at $\alpha=\alpha_0(\theta)$ (see text); $\tilde{\alpha}_c(0.8)=0.442$, $\alpha_0(0.8)=0.073$.

borhood of α_0. Recall that $\sqrt{\alpha r}$ represents the width of the Gaussian distribution of the renormalized noise in the local field in the SCSNA scheme. We can see that with α approaching α_0 from above, the width $\sqrt{\alpha r}$ of noise distribution tends to 0.

The clue to this anomalous behavior of r is as follows. Since we know $m<1$ and $|\Gamma|<m$ near α_0 by numerically solving (4.10), it turns out from (4.9) and (4.10) that $z_1, z_2, z_3 \to -\infty$ and $m \to N[-\infty, z_4] < 1$ as $r \to 0$. Accordingly, we have $z_4=(\theta-\Gamma/2-m)/\sqrt{\alpha r} < \infty$ and then

$$m \to \theta - \frac{\Gamma}{2} \quad (r \to 0) . \tag{4.20}$$

Further noting that in the limit $r \to 0$, $U\sqrt{\alpha r} \to -(1/\sqrt{2\pi})e^{-z_4^2/2}$ and hence $U \to -\infty$ we have

$$\Gamma = \frac{\alpha U}{1-U} \to -\alpha . \tag{4.21}$$

Equations (4.20) and (4.21) give

$$m = \theta + \frac{\alpha}{2} . \tag{4.22}$$

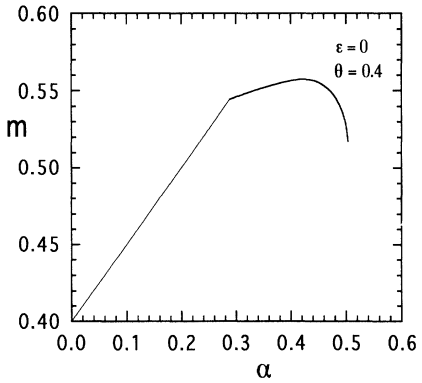

FIG. 16. Plot of m against α for $\theta=0.4$ ($\epsilon=0$) showing $\tilde{\alpha}_c(0.4)=0.503$, $\alpha_0(0.4)=0.289$.

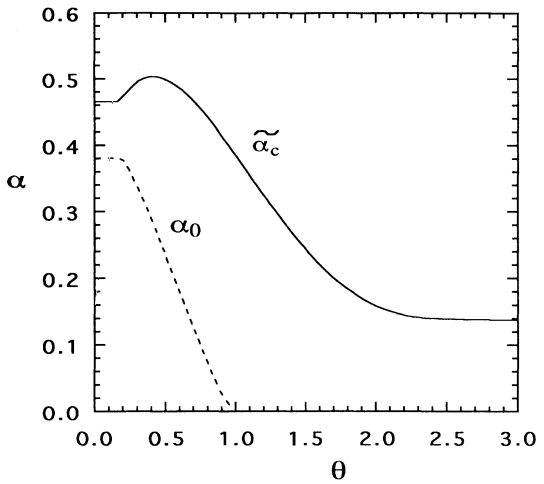

FIG. 17. Plots of $\tilde{\alpha}_c$ and α_0 as a function of θ when $\epsilon=0$. The α_0 curve manifests itself for $\theta \leq 1$. Whereas the storage capacity α_c is given by $\tilde{\alpha}_c$ in the case of $\theta \gtrsim 1$, the former gets decreased from the latter due to the occurrence of instability when $\theta \lesssim 1$.

In fact, we confirm this by looking at Figs. 15 and 16; the curve representing $m(\alpha)$, i.e., the solution to (4.10), disappears upon crossing the straight line given by (4.22). Since z_4 was determined by applying the Maxwell rule in Fig. 11(a), the relation (4.22) associated with the occurrence of the anomalous behavior should be just the consequence of the rule [compare (4.22) with the result of a finite pattern case (4.6) or the result of a similar anomalous behavior exhibited by the case of $\epsilon=1$ below (4.26)].

We turn to the case of $\alpha<\alpha_0$ where the standard type of solution with $m\neq 0$, $r\neq 0$ of the SCSNA can no longer exist. Let us assume that $r=0^+$ still holds together with $U \to -\infty$ when $\alpha<\alpha_0$. Then, repeating the discussion

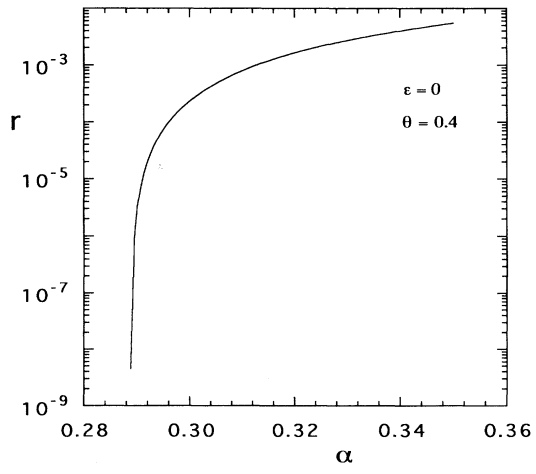

FIG. 18. Log plot of r against α in the vicinity of α_0, when $\theta=0.4$ with $\alpha_0=0.289$. As α tends to α_0, r is seen to approach 0.

above, we see that (4.22) follows. Although the set of Eqs. (4.10) as a whole does not seem to work in the limit $r \to 0$, the equation for m (4.10a) can be considered to hold even in this limit:

$$\theta + \frac{\alpha}{2} = N[-\infty, z_4] \ . \tag{4.23}$$

This equation gives z_4, which determines the renormalized output $Y(z)$ for $\alpha \leq \alpha_0$. The validity of (4.23) as well as (4.22) is confirmed by the results of numerical simulations of (2.1), which will be discussed later. When (4.23) holds, it may also be reasonable to expect that the spin-glass order parameter q obeys the relation $q = \theta + \alpha/2 = m$, which is implied by (4.10b) in the limit $r \to 0$. We note here that if r were exactly zero, (4.22) would not hold anymore, and instead $m = \theta/(1-\alpha)$. One must distinguish between $r=0$ and $r \to 0$. For this reason, we refer to the $\alpha \leq \alpha_0$ phase as the $r = 0^+$ phase.

In the $r = 0^+$ phase the tolerance overlap g (4.18) and (4.19a) becomes

$$g = 1 \ , \tag{4.24}$$

because $z_0, z_2, z_3 \to -\infty$. This implies that the network with $\alpha \leq \alpha_0$ ensures the complete retrieval of memory. It is surprising that *even with extensively many patterns stored, the network still exhibits the property of a perfect recall of memory.* The very reason for this phenomenon is that the residual part of the local field $\sum_{\mu>1}^{\alpha N} \xi_i^{(\mu)} m^{(\mu)}$ vanishes for $\alpha \leq \alpha_0$: besides $r = 0^+$, we see from (4.21) and (2.12) that $\gamma = 0$. Note, however, the difference between the values of m in (4.22) for $\alpha \neq 0$ and in (4.6) for $\alpha = 0$ (a finite number of patterns). The absence of the self-couplings, i.e., $\epsilon = 0$ in the case of extensively many patterns turns out to be responsible for the difference, because the limiting value $-\alpha$ of Γ in (4.21) originates from the second term of (2.12) in the present case. Then it is also noted that $\alpha/2$ in (4.22) is just a result of the application of the Maxwell rule.

In view of the qualitative change at $\alpha = \alpha_0$ of the statistical property of the associative memory recall, we may refer to the point $\alpha = \alpha_0$ at which the two types of retrieval states with $r \neq 0$ and $r = 0^+$ exchange each other as a phase-transition point, although no symmetry breaking seems to be involved there. We depict in Fig. 19 the tolerance overlap g plotted against α for $\theta = 0.8$. The qualitative change in the memory retrieval process, however, can be seen to occur not abruptly but continuously when α crosses the crossover point $\alpha = \alpha_0$. The θ dependence of the α_0 without taking into account the stability problem was already shown in Fig. 17.

2. $\epsilon = 1$

We consider the case of $\epsilon = 1$ to observe the effects of the self-couplings on the enhancement of the storage capacity and on the behavior of the phase transition. A more general case of $\epsilon > 0$ will be briefly discussed later.

a. Enhancement of the storage capacity due to the self-couplings. Setting $\epsilon = 1$ yields

$$\Gamma = \frac{\alpha}{1-U} \ , \tag{4.25}$$

which is positive as long as $U < 1$, and hence cases III and IV are to be applied. Solving (4.12) or (4.14) for the standard type of solution $m \neq 0$, $r \neq 0$ as before, we can obtain the value of $\bar{\alpha}_c$ defined as the upper bound of α ensuring the existence of retrieval solutions. Figure 20 shows $m(\alpha)$ curves for $\theta = 1.2$, 0.8, and 0.4, respectively. As in the case of $\epsilon = 0$, when $\theta < 1$ the standard type of solution with $r \neq 0$ of the SCSNA can be allowed only for α between the two critical values: $\alpha_0(\theta) < \alpha < \bar{\alpha}_c(\theta)$. Since the retrieval solutions with $\epsilon = 1$ are confirmed to be stable by numerical simulations, the $\bar{\alpha}_c$ turns out to equal the storage capacity.

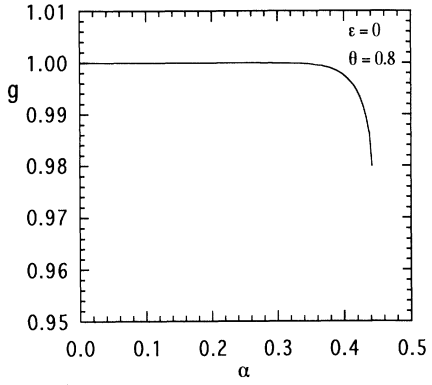

FIG. 19. Plot of the tolerance overlap g against α for $\theta = 0.8$ and $\epsilon = 0$. Note that $g = 1$ exactly holds for $0 \leq \alpha \leq \alpha_0(0.8) = 0.073$.

The storage capacity α_c is presented as a function of θ in Fig. 21. The α_c exhibits a broad peak at a small value of θ: $\alpha_c^{\max} \cong 0.775$ at $\theta \cong 0.27$. If the problem of the appearance of spurious states can be put aside, we see by comparing the present case with the case $\epsilon = 0$ (Fig. 17) a remarkable enhancement of the storage capacity due to the self-couplings which amounts to as much as about a five times larger value than the well-known value of 0.138 for the original Hopfield model. It should be noted that the effect of the self-couplings is to increase the stability of the retrieval solutions and spurious ones as well. Indeed, the fact that $\bar{\alpha}_c = \alpha_c$ is attributed to the suppression of instability exhibited by the retrieval solutions under no self-couplings.

b. Phase transition at $\alpha = \alpha_0$ and the behavior below α_0. When α approaches the lower critical value α_0 from above in the case of $\theta < 1$ with $\epsilon = 1$, r of the standard solution to (4.12) is found to tend to 0, and the phase transition occurs at α_0 as in the case $\epsilon = 0$. It is reasonable to expect that the equilibrium state of the networks below the transition point is characterized by the vanishing noise $r = +0$. Assuming $r \to +0$ in (4.11b) and (4.12), we have $z_0, z_1, z_2 \to -\infty$ and $|U| \to \infty$, and hence from (4.25) $\Gamma \to 0$. Then we can postulate that $z_4 = (\theta - m)/\sqrt{\alpha r}$ and $z_3 = z_4 - \Gamma/\sqrt{\alpha r}$ remain to be finite. Accordingly, it follows that

$$m \to \theta \quad (r \to 0+) \ . \tag{4.26}$$

Unlike in the case of $\epsilon = 0$ we can formally deal with the SCSNA equations (4.12) for the description of the property of the phase with $\alpha \leq \alpha_0$. Suppose

$$w \equiv \lim_{r\to 0}(z_4 - z_3) = \lim_{r\to 0} \frac{\Gamma}{\sqrt{\alpha r}} \ . \tag{4.27}$$

Taking the limit $r \to 0+$ of (4.12a) and using (4.26) together with (4.27) yields

$$\theta = N[-\infty, z_4 - w] + \frac{z_4 N[z_4 - w, z_4]}{w} + \frac{1}{w\sqrt{2\pi}}\{e^{-z_4^2/2} - e^{-(z_4-w)^2/2}\} \ . \tag{4.28}$$

Furthermore, combining (4.12b) and (4.12c) in the limit $r \to 0+$, we obtain

$$\frac{N[z_4 - w, z_4]^2}{\alpha} = w^2 N[-\infty, z_4 - w] + (1 + z_4^2) N[z_4 - w, z_4] + \frac{2z_4}{\sqrt{2\pi}}\{e^{-z_4^2/2} - e^{-(z_4-w)^2/2}\} - \frac{1}{\sqrt{2\pi}}\{z_4 e^{-z_4^2/2} - (z_4 - w) e^{-(z_4-w)^2/2}\} \ . \tag{4.29}$$

These equations yield w and z_4, from which the renormalized output $Y(z)$ will be determined. Note, however, that the solution w and z_4 does not satisfy either of the equations (4.12b) or (4.12c) itself under such a scaling as taken above for w and z_4 in the limit $r \to 0+$. A more systematic derivation of the above equation is given in Appendix B, where the $r = 0^+$ phase below α_0 in the case of $\epsilon = 1$ will be shown to be describable in terms of a certain limit of the SCSNA equations (4.12).

We have drawn the line $m = \theta$ in Figs. 20(b) and 20(c) to show that the $m(\alpha)$ curve corresponding to the standard type of solution with $r \neq 0$ disappears upon crossing the line, giving birth to the $r = 0^+$ "solution" represented by the line $m = \theta$ itself. Figures 22(a) and 22(b) display the behavior of the solutions to the set of Eqs. (4.28) and (4.29) for changing α in terms of $1/w$ and z_4/w, respectively, in the case of $\theta = 0.4$ ($\epsilon = 1$). The irrelevant solution is represented by the dash-dotted-line and the relevant one by the solid line. In accordance with the fact that the $r = 0^+$ phase occurs for $\alpha \leq \alpha_0$, the two solutions are seen to terminate at $\alpha = \alpha_0$ [$\alpha_0(\theta = 0.4) = 0.409$]. The two quantities $1/w$ and z_4/w, respectively, represent the width and output V_0 yielding the peak of the output distribution $\tilde{P}(V)$, which will be defined and discussed later.

For the tolerance overlap g of (4.16) in the case of

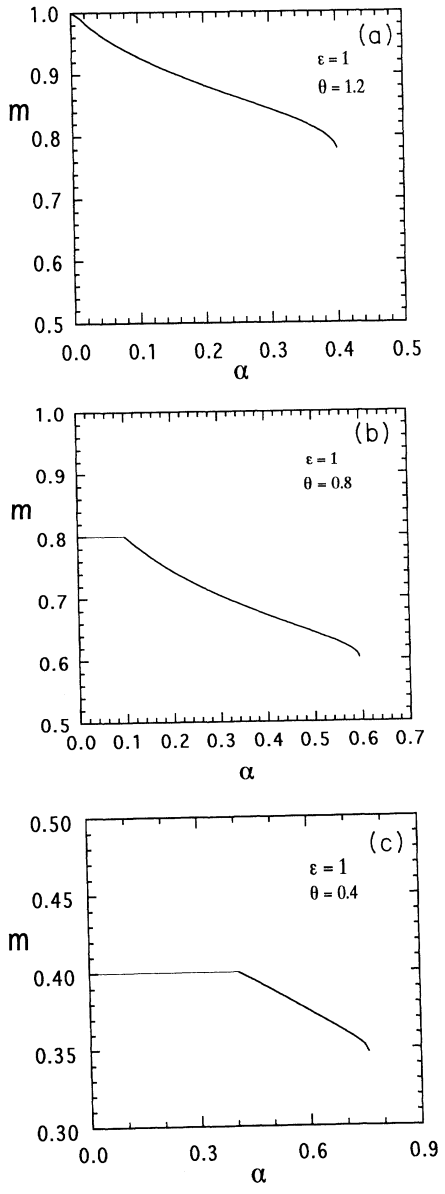

FIG. 20. Plot of the order-parameter overlap m as a function of α for (a) $\theta = 1.2$, (b) $\theta = 0.8$, and (c) $\theta = 0.4$, when $\epsilon = 1$. The thick curves represent $m(\alpha)$ given by the standard type of retrieval solutions with $r \neq 0$, whereas the thin lines in (b) and (c) give $m(\alpha)$ implied by the $r = 0^+$ solution [see Eq. (4.26)].

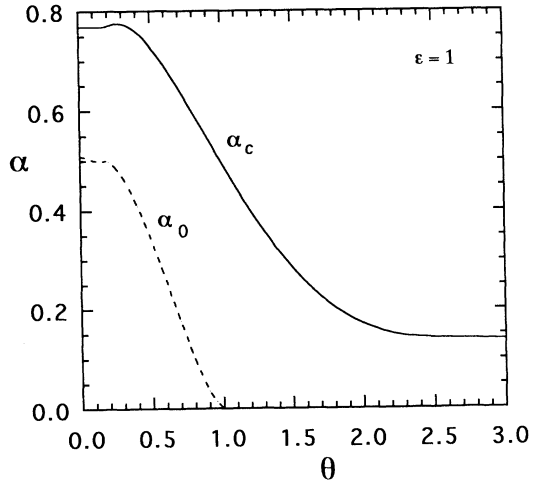

FIG. 21. Phase diagram on the θ-α plane displaying the θ dependence of the storage capacity α_c together with $\alpha_0(\theta)$ for $\epsilon = 1$.

$\Gamma > 0$, immediately follows the expression (4.18) from the fact that the local field is not allowed to vanish, i.e., $h \neq 0$. We see that $g = 1$ holds for $\alpha \leq \alpha_0$, implying that memory retrieval without errors is also possible in the case of $\epsilon = 1$. The dependence of the α_0 on θ is drawn in the phase diagram on the θ-α plane already given in Fig. 21.

Before passing, we briefly discuss a general case of $\epsilon > 0$. We depict examples of the ϵ dependence of the storage capacity α_c as well as of the values of $\bar{\alpha}_c$ for fixed values of θ in Fig. 23 ($\theta = 0.4$ and 1.0). An appreciable difference between the α_c and $\bar{\alpha}_c$ can be seen for small values of ϵ. The effect of the self-couplings turns out to increase the stability of the retrieval solutions to the SCSNA order-parameter equations. As ϵ is increased from $\epsilon = 0$, the α_c is seen to increase to attain its maximum value at a certain value of ϵ and afterwards to decrease with a further increase of ϵ. Such nonmonotonic behavior of the storage capacity accompanied by the change in ϵ turns out not to go parallel with the case of the center-cutoff-type transfer functions in the preceding section, although a qualitative explanation for the difference remains to be given. As for the occurrence of the phase transition involving the disappearance of the noise in the local field in the case of $\theta < 1$, networks with $0 < \epsilon < 1$ were found to exhibit qualitatively the same

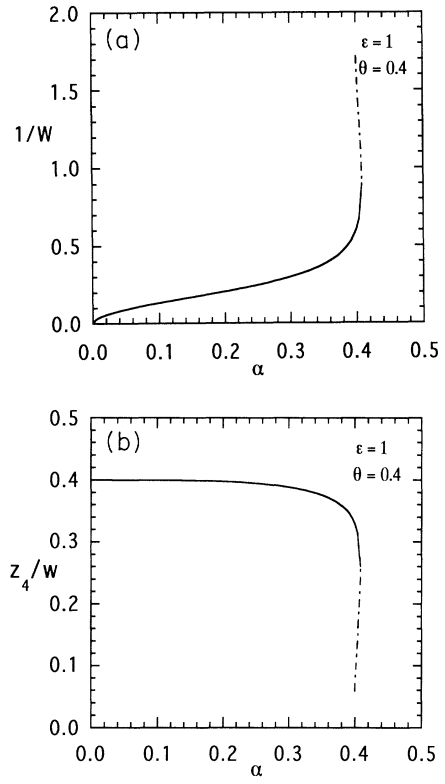

FIG. 22. Behavior of the solutions to the set of Eqs. (4.28) and (4.29) describing the $r = 0^+$ phase with $\epsilon = 1$. (a) Plot of $1/w$ against α for $\theta = 0.4$, (b) Plot of z_4/w against α for $\theta = 0.4$. The relevant solution (the solid line) and irrelevant one (dash-dotted line) are seen to merge with each other to terminate at $\alpha = \alpha_0$ (=0.409).

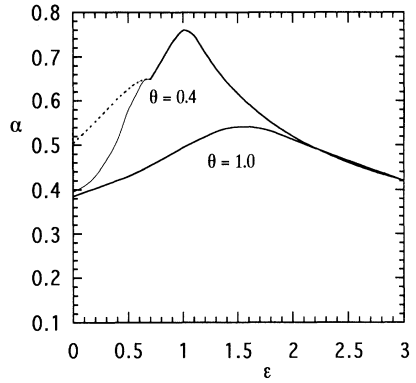

FIG. 23. Plots of α_c (solid) and $\bar{\alpha}_c$ (dotted) against ϵ for $\theta = 0.4$ and 1.0. The thin line was determined numerically, and the thick line implies $\bar{\alpha}_c = \alpha_c$. The deviation of α_c from $\bar{\alpha}_c$ is due to the occurrence of instability of the retrieval solutions.

behavior as that of $\epsilon = 0$. However, when $\epsilon > 1$, there occurs no such phase transition. We can see this quite easily using (4.12) and (4.14). (Note that $\Gamma > 0$ for $\epsilon > 1$.) Suppose $r = 0^+$ occurs for $\alpha \neq 0$ in (4.12) or (4.14). Then $|U| \to \infty$ follows as before, but Γ turns out to remain nonzero [i.e., $\alpha(\epsilon - 1)$] this time. This leads to a contradiction in (4.12c) or (4.14c). The vanishing of the noise occurs only in the limit $\alpha \to 0$.

C. Local field and output distributions

The occurrence of the new type of phase transition which arises from the vanishing of the residual part of the local field (i.e., $r \to 0+$) can be more directly seen by examining the local field distribution $P(h)$. It is defined as

$$P(h) = \left\langle \frac{\exp(-z^2/2)}{\sqrt{2\pi}} \frac{dz}{dh} \right\rangle_{\xi} , \tag{4.30}$$

which is quite easy to evaluate using the renormalized local field $h(\xi, z)$ together with the renormalized output $Y(\xi, z)$.

In the case of $-2\theta < \Gamma < 0$ (case II) and $0 < \Gamma < \theta$ (case III), which covers a large region of the retrieval phase of interest in the θ-α phase diagram for $\epsilon = 0$ (Fig. 17) and $\epsilon = 1$ (Fig. 21), respectively, the local field distribution is given as follows. For $-2\theta < \Gamma \leq 0$

$$P(h) = \begin{cases} N\left[\dfrac{m+\Gamma}{\sqrt{\alpha r}}, \dfrac{m-\Gamma}{\sqrt{\alpha r}}\right]\delta(h) + P_1(h), & |h| < \theta - \dfrac{|\Gamma|}{2} \\ P_2(h), & |h| > \theta + \dfrac{|\Gamma|}{2} \\ 0, & \theta - \dfrac{|\Gamma|}{2} < |h| < \theta + \dfrac{|\Gamma|}{2} \end{cases} , \tag{4.31}$$

and for $0 < \Gamma < \theta$

$$P(h) = \begin{cases} \Theta(|h| - \theta)P_2(h) + \Theta(-|h| + \theta)P_1(h) \\ \qquad + \omega\delta(|h| - \theta) , & \Gamma \leq |h| \\ 0, & \Gamma > |h| , \end{cases}$$

(4.32)

where

$$P_1(h)=\frac{1}{2\sqrt{2\pi\alpha r}}\left\{\exp\left[-\frac{(|h|-m-\Gamma)^2}{2\alpha r}\right]+\exp\left[-\frac{(|h|+m-\Gamma)^2}{2\alpha r}\right]\right\},$$

$$P_2(h)=\frac{1}{2\sqrt{2\pi\alpha r}}\left\{\exp\left[-\frac{(h-m)^2}{2\alpha r}\right]+\exp\left[-\frac{(h+m)^2}{2\alpha r}\right]\right\}, \quad (4.33)$$

$$\omega=\tfrac{1}{2}\{N[z_3,z_4]-N[z_2,z_1]\},$$

with z_1, z_2, z_3, and z_4 given by (4.11b), and $\Theta(x)$ represents the Heaviside function [$\Theta(x)=1$ for $x\geq 0$ and $\Theta(x)=0$ for $x<0$].

We immediately notice that the local field distribution $P(h)$ is not Gaussian but piecewise of a sum of Gaussian distribution. The non-Gaussian behavior is a consequence of the ΓY term in the renormalized local field of analog neural networks, as was mentioned in Sec. II. In particular, clear evidence of the non-Gaussian property is the appearance of the forbidden gap in the $P(h)$; due to the Maxwell rule, the local field is forbidden to take its values in the interval of width $|\Gamma|$,

$$\theta-\frac{|\Gamma|}{2}<|h|<\theta+\frac{|\Gamma|}{2} \quad (4.34)$$

in the case of $-2\theta<\Gamma<0$, and in the interval $|h|<\Gamma$ in the case of $0<\Gamma<\theta$. We give, in Figs. 24 and 25, respectively, some examples of $P(h)$ computed in the case of $\theta=0.8$ and 0.4 for different values of α with $\epsilon=0$, for which $-2\theta<\Gamma<0$ holds. In addition to the appearance of the forbidden gap in the local field distribution, we clearly see that the narrowing of the width of the distribution occurs in accordance with $r\to 0$, when α approaches α_0. When $\alpha\leq\alpha_0$, taking the limit $r\to 0$ of (4.31) and using (4.22) and (4.23) one has

$$P(h)=\frac{\theta+\alpha/2}{2}\delta\left[|h|-\left[\theta-\frac{\alpha}{2}\right]\right]+\frac{1-\theta-\alpha/2}{2}\delta\left[|h|-\left[\theta+\frac{\alpha}{2}\right]\right]. \quad (4.35)$$

Figure 26 displays examples of the profile of the $P(h)$ given by (4.32) for different values of α when $\theta=0.4$ with $\epsilon=1$. It is noted that the overall spreading of the distribution is quite narrow compared with the case of $\epsilon=0$, owing to the existence of the δ-function component located at $|h|=\theta$. The width of the remaining broader component of the distribution is seen to get narrower in accordance with $r\to 0$, as α approaches α_0. When $\alpha\leq\alpha_0$, it turns out that the $P(h)$ is concentrated on $|h|=\theta$ (though not displayed here).

In such a case where the local field distribution is independent of α ($\alpha\leq\alpha_0$ and $\epsilon=1$), it is of use to consider the output distribution which varies with α. The output distribution, in general, helps a lot to observe more directly the shape of the renormalized output $Y(z)$ which plays a central role in the SCSNA under the functioning of the output proportional term ΓY.

Letting

$$V_i=\xi_i^{(1)}x_i[=\xi_i^{(1)}F(u_i)], \quad i=1,\ldots,N, \quad (4.36)$$

we define the distribution $\tilde{P}(V)$ of the scaled output $\{V_i\}$ as in the case of the local field distribution $P(h)$. [Replace h in (4.30) with $V(\xi,z)\equiv\xi Y(\xi,z)$.] Explicit expres-

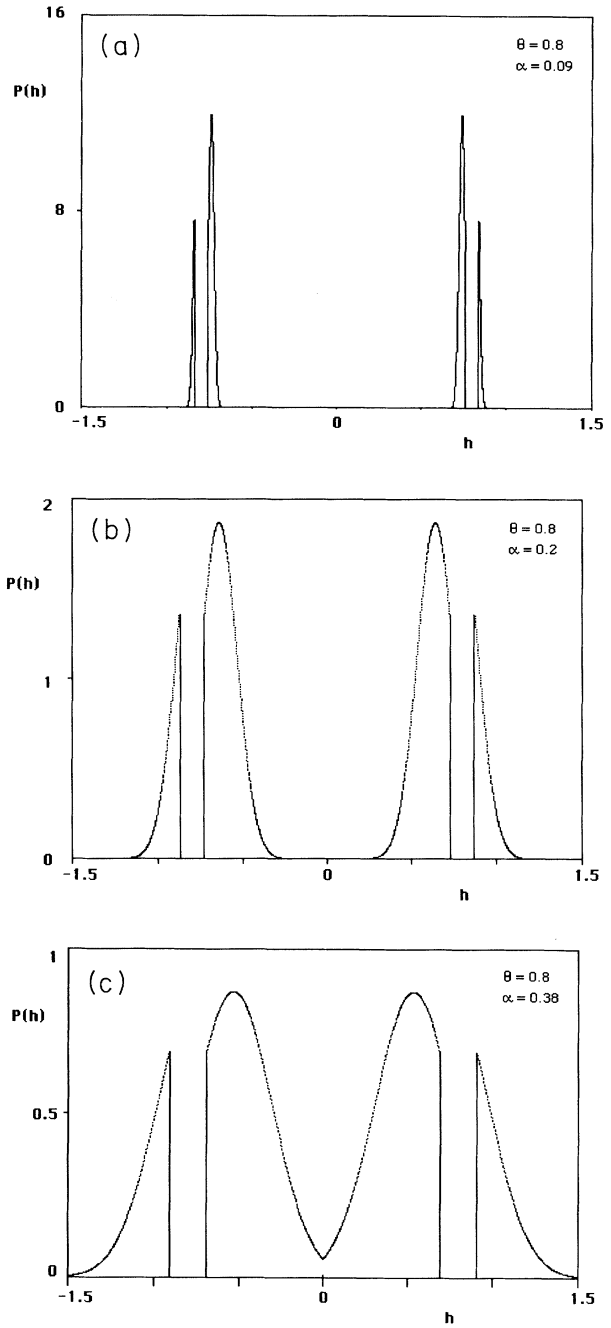

FIG. 24. Local field distribution $P(h)$ computed from (4.31) with $\epsilon=0$ for $\theta=0.8$, for several values of α: (a) $\alpha=0.09$, (b) $\alpha=0.2$, (c) $\alpha=0.38$.

sions for the output distribution $\tilde{P}(V)$ in the case of $-2\theta<\Gamma\le 0$ and $0<\Gamma<\theta$ are given as follows.

When $-2\theta<\Gamma\le 0$,

$$\tilde{P}(V)=I_{[-1,1]}(V)\frac{\Gamma}{\sqrt{2\pi\alpha r}}\exp\left[-\frac{(\Gamma V+m)^2}{2\alpha r}\right] +N[z_3,z_4]\delta(V-1)+\{1+N[z_4,z_1]\}\delta(V) +N[z_1,z_2]\delta(V+1)\ , \tag{4.37}$$

with z_1, z_2, z_3, and z_4 being given by (4.9b), and $I_{[-1,1]}(V)$ denoting the indicator function of the interval $[-1,1]$.

In particular, for $\alpha\le\alpha_0$ with $r=0^+$ and $\Gamma=-\alpha$, the $\tilde{P}(V)$ turns out to consist of the δ-function components alone:

$$\tilde{P}(V)=N[-\infty,z_4]\delta(V-1)+N[z_4,\infty]\delta(V)\ . \tag{4.38a}$$

Here we noted that the continuous component in (4.37) vanishes, because $-2\theta<\Gamma\le 0$ implies $\alpha<2\theta$. Noting $m=\int_{-\infty}^{\infty}V\tilde{P}(V)dV$ together with (4.22), we see that (4.23) is recovered. Then (4.38a) is rewritten as

$$\tilde{P}(V)=\left[\theta+\frac{\alpha}{2}\right]\delta(V-1)+\left[1-\theta-\frac{\alpha}{2}\right]\delta(V)\ . \tag{4.38b}$$

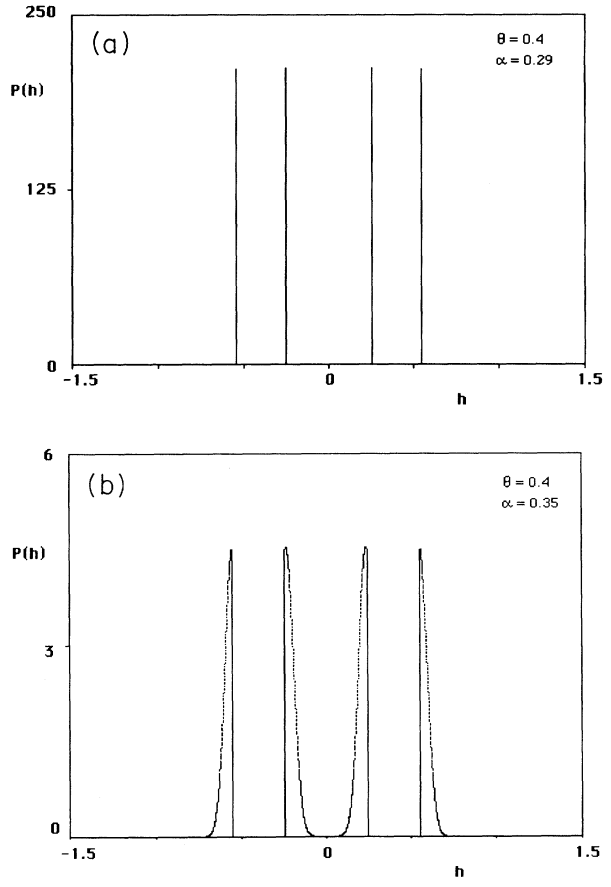

FIG. 25. Same as Fig. 24 for $\theta=0.4$: (a) $\alpha=0.29$, (b) $\alpha=0.35$.

When $0<\Gamma<\theta$,

$$\tilde{P}(V)=I_{[0,1]}(V)\frac{\Gamma}{\sqrt{2\pi\alpha r}}\exp\left[-\frac{[\Gamma V-(\theta-m)]^2}{2\alpha r}\right] +I_{[-1,0]}(V)\frac{\Gamma}{\sqrt{2\pi\alpha r}}\exp\left[-\frac{[\Gamma V+(\theta+m)]^2}{2\alpha r}\right] +N[z_0,z_3]\delta(V-1)+\{1+N[z_4,z_1]\}\delta(V) +N[z_2,z_0]\delta(V+1)\ , \tag{4.39}$$

with z_0, z_1, z_2, z_3, and z_4 given by (4.11b).

Of particular interest here is the case $\alpha\le\alpha_0$ with $\epsilon=1$ and $\theta<1$. Noting in the limit $r\to 0+$ (4.27) and so on, the above $\tilde{P}(V)$ turns out to take the form

$$\tilde{P}(V)=I_{[0,1]}(V)\frac{w}{\sqrt{2\pi}}\exp\left[-\frac{w^2(V-z_4/w)^2}{2}\right] +N[-\infty,z_4-w]\delta(V-1)+N[z_4,\infty]\delta(V)\ , \tag{4.40}$$

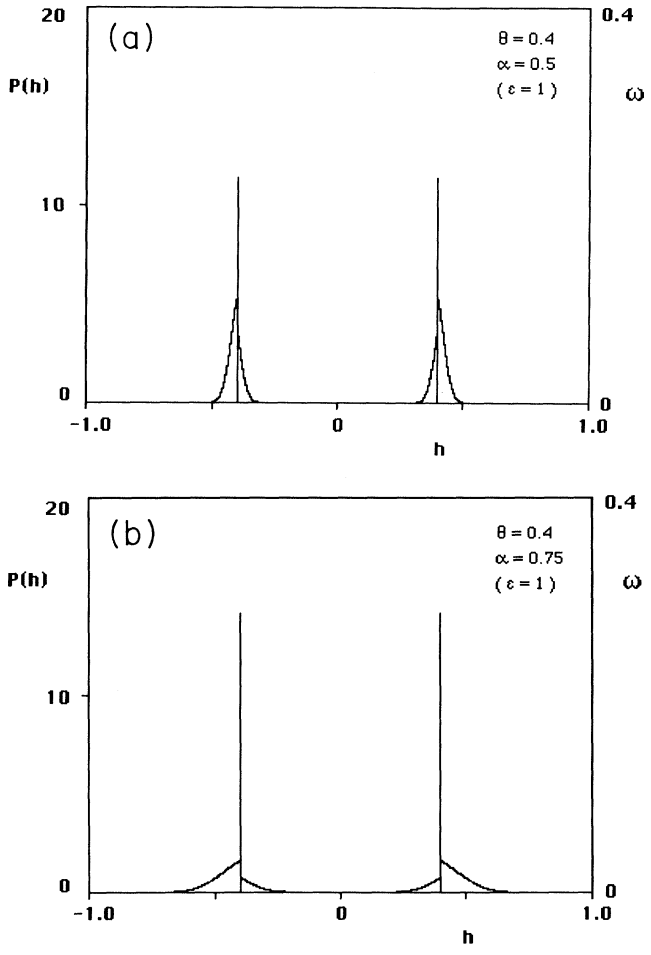

FIG. 26. Local field distribution $P(h)$ given by (4.32) with $\epsilon=1$ for $\theta=0.4$, for several values of α: (a) $\alpha=0.5$, (b) $\alpha=0.75$. The right-hand side ordinate represents the magnitude ω of the δ-function components of the local field distribution.

where w and z_4 are determined by (4.28) and (4.29). Although below the transition point α_0 ($\epsilon=1$) the local field distribution $P(h)$ is concentrated on $|h|=\theta$, the $\tilde{P}(V)$ still has a continuous component taking a Gaussian form with variance $1/w^2$ and mean z_4/w. Figure 27 depicts the profile of $\tilde{P}(V)$ given by (4.40) for $\theta=0.4$ and $\alpha=0.25$ together with the one given by (4.39) for $\theta=0.4$ and $\alpha=0.75$. Note that the continuous component of the output distribution arises from the slant part ($z_3 \le z \le z_4$) of the renormalized output $Y(z)$ in Fig. 12(b). The dependence of the variance $1/w^2$ and mean z_4/w on the loading rate α was already given in Fig. 22. From (4.28) and (4.29) we can easily see that as α approaches 0, $z_4/w \to \theta$ and $1/w^2 \to \alpha\theta^2$.

D. Numerical simulations

We conducted numerical simulations to confirm the theoretical results of the SCSNA for the networks of nonmonotonic neurons presented in the preceding section. Most of the numerical simulations performed were on the networks of N neurons with N ranging from 100 to 700, where the sets of differential equations (2.1a) or (2.1b) with the transfer function (4.1) or the one having a smooth parameter δ were solved for a variety of combinations of initial conditions and parameters involved in the models by means of the Runge-Kutta method with time step $\Delta t=0.01$ or 0.025 and the number of steps n sufficiently large for its convergence ($n \lesssim 1500$). The target was set particularly on examining the stability of the retrieval solutions given by the SCSNA order-parameter equations, the critical storage capacity α_c, the effect of the self-couplings, and the occurrence of the new type of phase transition associated with the onset of the perfect recall of memory. Apart from the stability problem in which the occurrence of instability makes α_c smaller than $\bar{\alpha}_c$ for small values of θ and ϵ as is shown below, the results of the simulations are in quite satisfactory agreement with those of the SCSNA, confirming the validity of the SCSNA itself together with the claimed prescription of the Maxwell rule.

Before presenting the simulation results obtained, we here note the use of the transfer functions (4.1) exhibiting jumps at $u=\pm\theta$ as well as $u=0$ in the numerical integrations of (2.1). As is previously mentioned of the treatment of the jumps of the transfer functions, numerical simulations, in general, have to be carried out on the networks having transfer functions with a very small smoothing parameter δ in Fig. 9(a), except for the case in

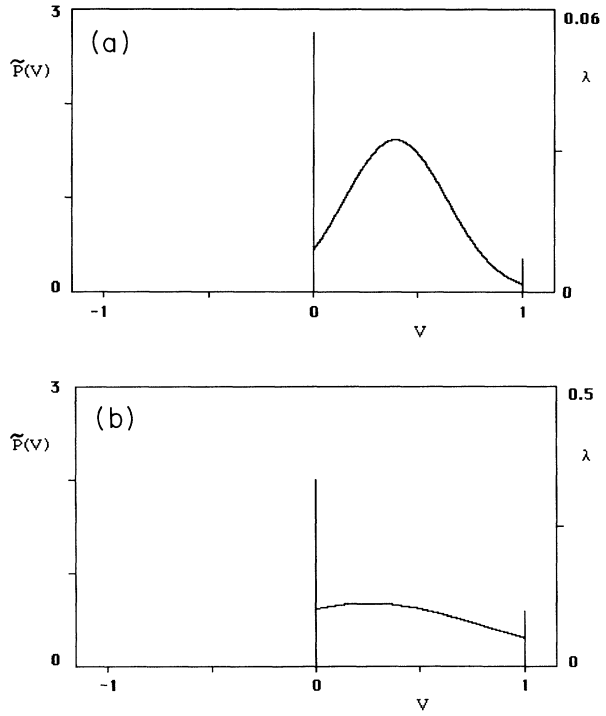

FIG. 27. Output distribution $\tilde{P}(V)$ given by (4.39) or (4.40) with $\epsilon=1$ for $\theta=0.4$. The right-hand side ordinate represents the magnitude λ of the δ-function components of the output distribution, e.g., $\lambda(V=1)=N[-\infty, z_4-w]$ and $\lambda(V=0)=N[z_4, \infty]$ in the case of Eq. (4.40). (a) $\alpha=0.25$($r=0^+$ phase) [$\lambda(V=1)=7.14\times10^{-3}$, $\lambda(V=0)=5.50\times10^{-2}$, $\lambda(V=-1)=0$], (b) $\alpha=0.75$ [$\lambda(V=1)=9.92\times10^{-2}$, $\lambda(V=0)=3.32\times10^{-1}$, $\lambda(V=-1)=8.29\times10^{-4}$].

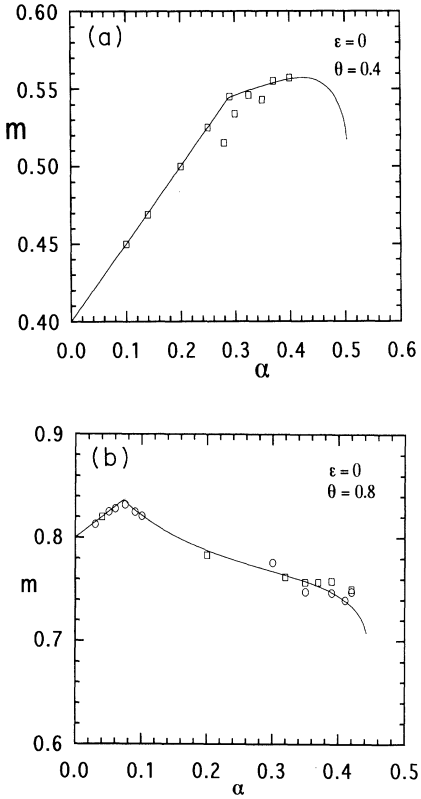

FIG. 28. Plot of m as a function of α for $\epsilon=0$ obtained from numerical simulations with various N together with the corresponding SCSNA result: (a) $\theta=0.4$ ($\alpha_0=0.289$, $\bar{\alpha}_c=0.503$, $\alpha_c \cong 0.40$), (b) $\theta=0.8$ ($\alpha_0=0.073$, $\bar{\alpha}_c=0.442$, $\alpha_c \cong 0.42$) (circle: $N=500$; rectangle: $N=200$). The upper bound for the existence of the stable retrieval solutions defines the storage capacity α_c.

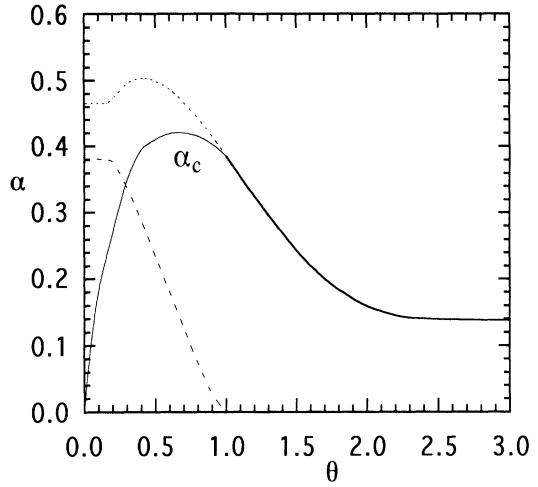

FIG. 29. Phase diagram on the θ-α plane showing the θ dependence of the storage capacity α_c for $\epsilon=0$ (solid line). The region $\alpha \leq \alpha_c$ represents the retrieval phase. The curves for $\bar{\alpha}_c$ and α_0 are reproduced from Fig. 17. The thin line which replaces the $\bar{\alpha}_c$'s for $\theta \lesssim 1$ (the dotted line) was determined numerically. The $r=0^+$ phase occurs in the region satisfying both $\alpha \leq \alpha_c$ (below the thin line) and $\alpha \leq \alpha_0$ (below the dashed curve).

which the SCSNA yields $\Gamma<0$. When $\Gamma<0$, the results with (4.1) (i.e., $F_{\delta_0\delta}$ in the limit δ_0, $\delta \to 0+$) can be recovered by use of the transfer functions $F_{0^+\delta}$ which are smoothed at $|u|=\theta$ with $\delta<|\Gamma|/2$.

We tried to compare between the use of the transfer functions $F_{0^+\delta}$ with exactly $\delta=0$ (jump) and $0<\delta \ll 1$ (smooth). Interestingly, it was found that in most cases use of $F_{0^+\delta}$ with $\delta=0$ yields almost the same results as obtained from transfer functions with $\delta \ll 1$, confirming the results of the SCSNA. We consider that it is a finite difference scheme introduced by the finite step size used in the numerical integrations for (2.1) that is responsible for preventing the updating dynamics with the jumps from losing its meaning, and hence for allowing one to view a sticking solution as a kind of equilibrium solution

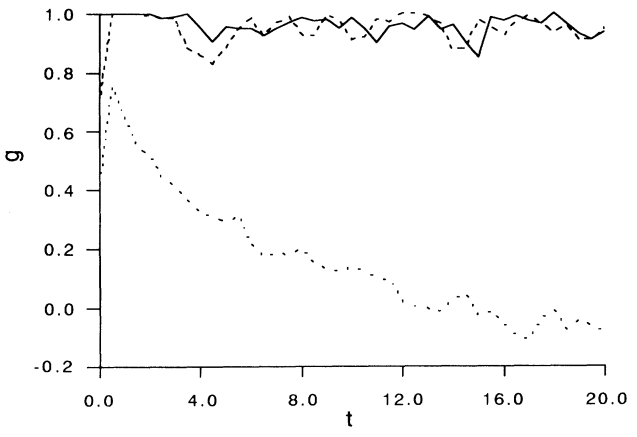

FIG. 30. Oscillatory instability exhibited by a neural network with $\alpha > \alpha_c$ for small θ. The time course of the retrieval process is expressed in terms of the tolerance overlap g: $\alpha=0.28$, $\theta=0.2$, $N=500$, and $\epsilon=0$.

for which the SCSNA is applicable.

A single major problem of using the $\delta=0$ transfer function was generated, when the local field distribution $P(h)$ was computed from the expression $h_i=\sum_j J_{ij}F(u_j)$ using the set of equations (2.1a) for membrane $\{u_i\}$. It seems that the sticking solution in that case together with the expression for h_i cannot properly reproduce the stationary local field distribution $P(h)$. Even in this case, however, the distribution of $\{u_i\}$ itself yields correct results for $P(h)$, which were also obtained using the set of equations (2.1b) for output $\{v_i\}$ together with $h_i=\sum_j J_{ij}v_j$.

1. *Case of $\epsilon=0$*

Figures 28(a) and 28(b), respectively, show the dependence of the order-parameter overlap m on the loading rate α for $\theta=0.4$ and 0.8 obtained from simulations with $N=200$ and 500. For comparison the theoretically obtained results are reproduced (thin lines) from Figs. 15 and 16. At first glance, we observe satisfactory agreement between the results of the SCSNA and those of the simulations below certain values of α, above which the retrieval solutions given by the SCSNA were found numerically not to attract dynamical flows with any initial conditions. It is noted that the occurrence of the new type of phase transition at α_0 and (4.22) describing the

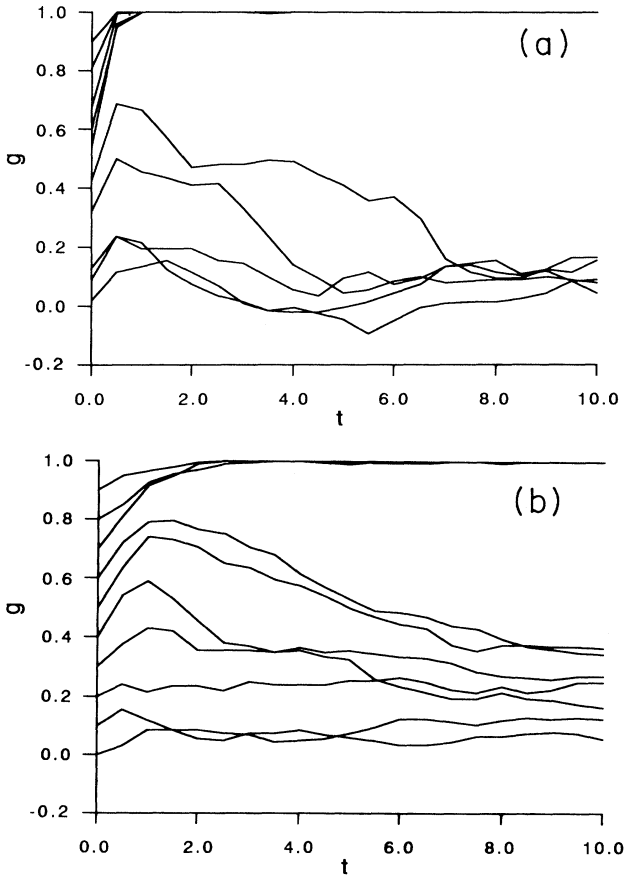

FIG. 31. Time course of the retrieval process in terms of g for networks in the retrieval phase ($N=500$): (a) $\alpha=0.3$, $\theta=0.3$; (b) $\alpha=0.3$, $\theta=1.1$.

behavior of m below α_0 are seen to be justified. The dependence of the spin-glass order parameter q on α below α_0 (though not shown here) was also confirmed to obey the relation $q=m=\theta+\alpha/2$ as is suggested by the theory, where the q is defined as $(1/N)\sum_{i=1}^{N} v_i^2(t=\infty)$ in numerical simulations.

The storage capacity α_c in such a case as given by $\theta=0.4$ and 0.8 should not coincide with $\bar{\alpha}_c$, but has to be determined numerically from the upper bound for the existence of the stable retrieval solutions. We given in Fig. 29 a phase diagram representing the θ dependence of the α_c together with the one reproduced from Fig. 17. Whereas the storage capacity α_c for $\theta \gtrsim 1$ is seen to equal $\bar{\alpha}_c$, the one for $\theta \lesssim 1$ gets reduced by an appreciable amount particularly at vanishing θ.

Figure 30 presents an example of the time evolutions of the tolerance overlap which was obtained when a network with small θ has α just outside the retrieval phase (i.e., $\alpha_c \leq \alpha \leq \bar{\alpha}_c$). We see that the occurrence of oscillatory instability with small amplitudes of oscillation indeed leads to the reduction of the storage capacity, making α_c smaller than $\bar{\alpha}_c$. The retrieval solution given by the SCSNA is considered to undergo a series of certain bifurcations including the Hopf bifurcations at or around the phase boundary representing the α_c. Note that due to the nonmonotonicity of the transfer function the existence of a Liapunov function cannot be expected any longer.

Examples of the retrieval process exhibited by the networks in the retrieval phase $\alpha \leq \alpha_c$, on the other hand, are shown in Fig. 31. Figures 31(a) and 31(b) display the time evolutions of the overlap g started with various initial values for the network with $\theta=0.3$ and $\alpha=0.3$ and for the one with $\theta=1.1$ and $\alpha=0.3$, respectively. Noting that the two cases have the same loading rate α, we see that the network with smaller θ is more tolerant of a de-

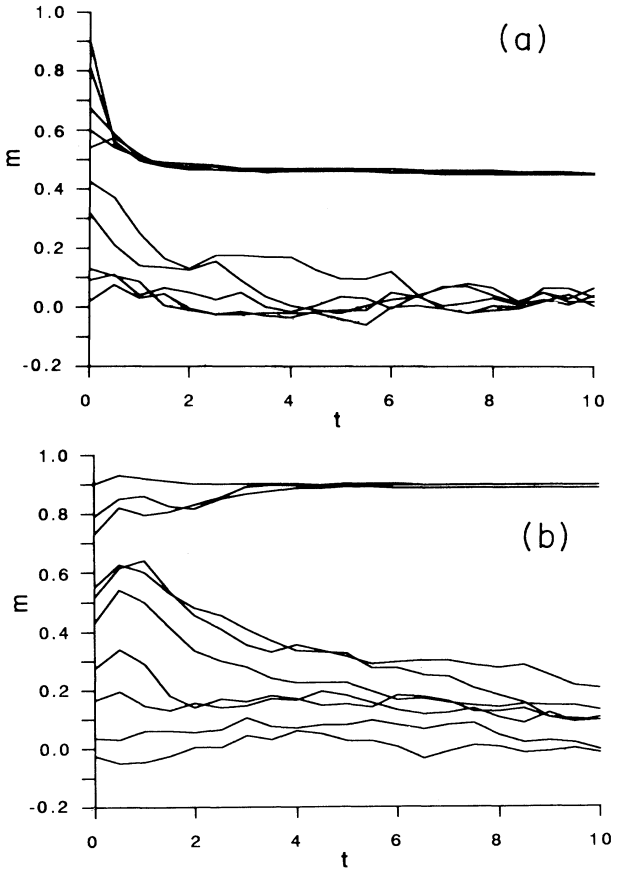

FIG. 32. Same as Fig. 31 but in terms of m. (a) $\alpha=0.3$, $\theta=0.3$; (b) $\alpha=0.3$, $\theta=1.1$.

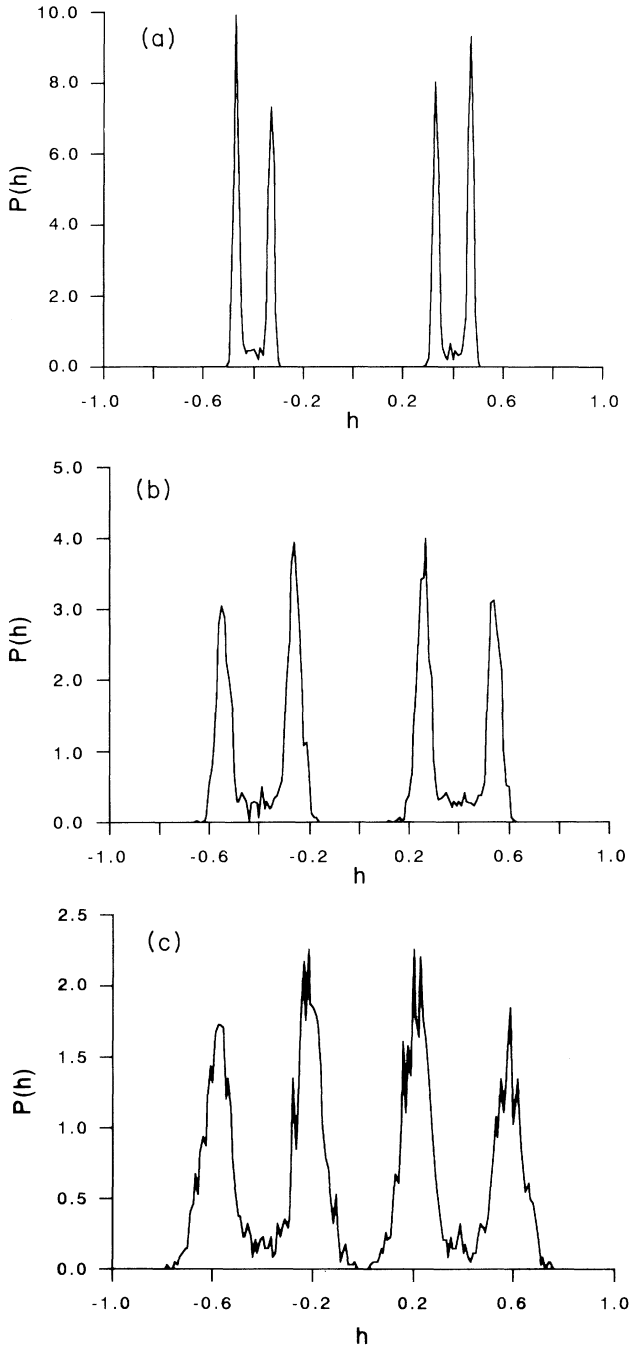

FIG. 33. Local field distribution $P(h)$ in the retrieval state ($\epsilon=0$) with $\theta=0.4$ for (a) $\alpha=0.14$, (b) $\alpha=0.29$, (c) $\alpha=0.35$ obtained from numerical simulations with $N=200$.

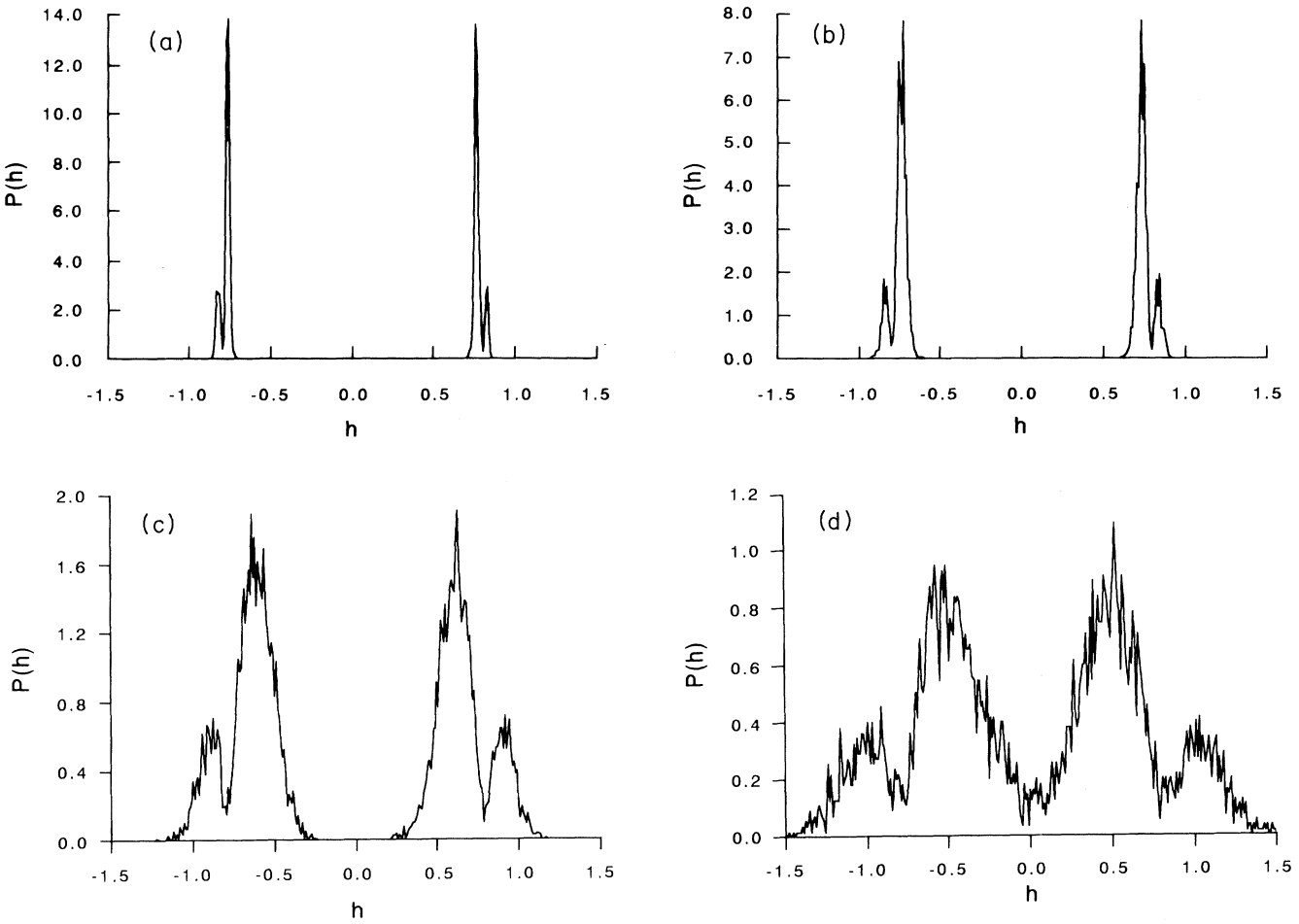

FIG. 34. Same as Fig. 33 with $\theta=0.8$: (a) $\alpha=0.06$, (b) $\alpha=0.09$, (c) $\alpha=0.2$, (d) $\alpha=0.38$ ($N=500$).

graded pattern given initially than the other one. It is noted that the retrieval state with $g=1$ attained in Fig. 31(a) is the $r=0^+$ state. We depict in Fig. 32 the time course of the retrieval process expressed in terms of m of Fig. 4. It is seen that the time required for an initial state of the network to settle into the retrieval state can be much reduced when expressed in terms of g. This implies that use of g is more appropriate in the networks with such transfer functions as the end-cutoff-type one not only as a reasonable measure to define the pattern overlap but also from the viewpoint of recall speed.

Let us turn to the local field distribution $P(h)$. Figures 33(a), 33(b), and 33(c) show the averaged histograms over an appropriate number of trials for the local field h_i's at equilibrium state of the network ($N=500$) with $\theta=0.4$ in the case of $\alpha=0.14$, 0.29, and 0.35, respectively, and Figs. 34(a), 34(b), 34(c), and 34(d) for $\alpha=0.06$, 0.09, 0.2, and 0.38, respectively, with $\theta=0.8$. Since $P(h)$ is symmetric with respect to $h=0$, i.e., $P(h)=P(-h)$, it will suffice to focus one's attention only to either half of the $P(h)$. As is suggested by the result of the SCSNA with $\epsilon=0$, each local field distribution in the figures is seen to be non-Gaussian and double peaked, although the slit with width $|\Gamma|$ which must be located at $|h|=\theta$ is not visible (compare with Figs. 24 and 25), probably due to the finiteness of N. Furthermore, as is observed particularly in Fig. 34 of the case of $\theta=0.8$, with α approaching α_0 the distribution gets more sharply peaked, and settles

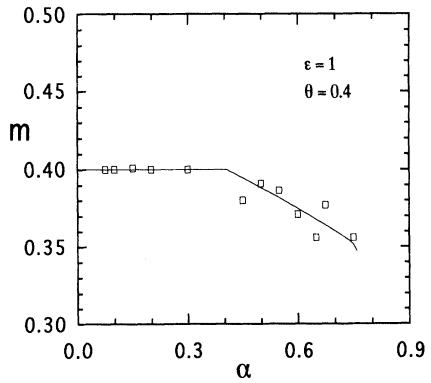

FIG. 35. Plot of m as a function of α obtained from numerical simulations for $\theta=0.4$ with $\epsilon=1$ together with the SCSNA result.

into two δ functions located at $|h|=\theta\pm|\Gamma|/2$ when $\alpha\leq\alpha_0$. We see that not only the profile but also the overall behavior with changing α of the local field distributions obtained from the simulations are qualitatively well explained by the results of the SCSNA.

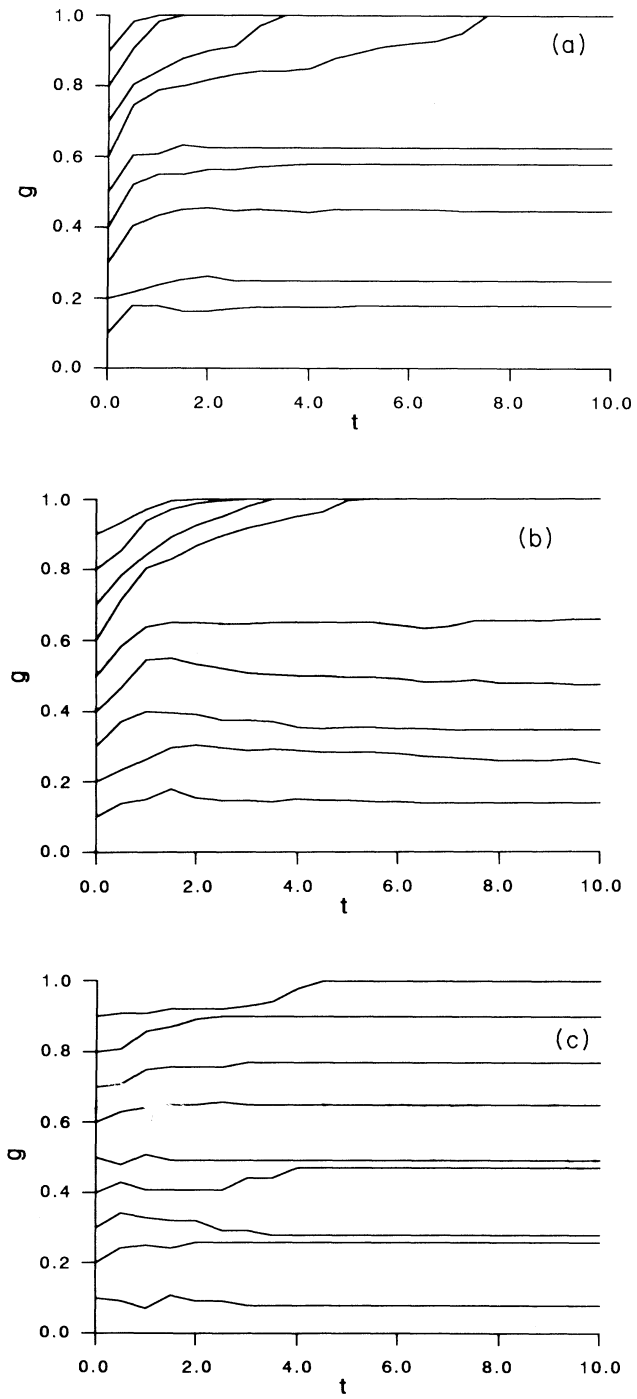

FIG. 36. Time course of the retrieval process in terms of the tolerance overlap g, when $\epsilon=1$ and $N=500$: (a) $\alpha=0.4$, $\theta=0.2$ ($r=0^+$ phase); (b) $\alpha=0.4$, $\theta=0.8$; (c) $\alpha=0.7$, $\theta=0.3$.

2. $\epsilon=1$

We depict in Fig. 35 a plot of m against α for $\theta=0.4$ which was obtained from simulations on the networks with the self-couplings $\epsilon=1$, together with the theoretical result of the SCSNA. Unlike the case of $\epsilon=0$, for the entire region of α below $\bar{\alpha}_c$ quite good agreement is found between the results of simulations and the theory, confirming the existence of the $r=0^+$ phase with the relation $m=\theta$. We now see that as a consequence of the stabilizing of the retrieval solutions to the SCSNA with a sufficient amount of the self-couplings, the storage capacity α_c with $\epsilon=1$ coincides with the value of $\bar{\alpha}_c$. The relation $\alpha_c=\bar{\alpha}_c$ holds for any θ. As was mentioned earlier, the effect of the self-couplings is to make the value of α_c approach the value of $\bar{\alpha}_c$ (see Fig. 23) by increasing the stability of the retrieval solutions and of spurious states as well. Figure 36 displays examples of the time course of the pattern retrieval process which are exhibited by the networks with α and θ specified by three different points in the α-θ phase diagram of Fig. 21, one of which belongs to the $r=0^+$ phase. Indeed, we notice that unlike the case of $\epsilon=0$ there seem to appear a number of spurious states especially in the vicinity of such a large value of α_c as ≈ 0.77; only the networks started with initial values of the tolerance overlap $g(0)$ close to 1 can settle into the retrieval state after some time, whereas the networks, if they fail to retrieve the stored patterns, are seen to be easily captured by spurious states with $g(\infty)$ near the initial value $g(0)$.

It will be possible, however, to control the value of ϵ so as to ensure high storage capacity while keeping the number of spurious states as small as possible. Such a choice of ϵ is given in Fig. 37, where the network with $\theta=0.4$ and $\epsilon=0.45$ is seen to yield an appreciably reduced number of spurious states under the loading rate of $\alpha=0.5$.

Turning to the problem of the statistical behavior of the networks with $\epsilon=1$, we depict in Figs. 38(a), 38(b), and 38(c) the local field distribution obtained from simulations with $N=200$ in the case of $\alpha=0.25$, 0.5, and 0.75, respectively, with $\theta=0.4$. The profile of the distribution

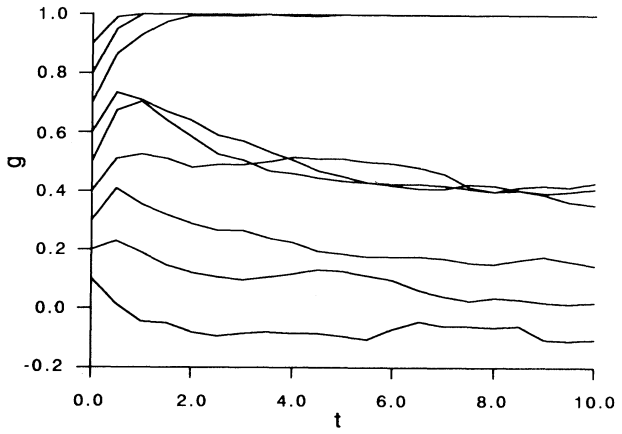

FIG. 37. Time course of the retrieval process in the case of $\epsilon=0.45$ for a network with $\alpha=0.5$ and $\theta=0.4$ ($N=500$).

for $\alpha > \alpha_0$ is seen to be composed of a sharp peak corresponding to a δ function and a more or less broad distribution, as is suggested by the theoretical result (4.32) of the SCSNA (see Fig. 26). The broad distribution, however, is seen to get narrower as α approaches α_0, and for α below α_0 the whole profile of the local field distribution turns out to be δ peaked at $|h|=\theta$. It should be noted that the local field distribution of $\epsilon=1$ is, as a whole, narrow for the largeness of the value of α. Compare the present case with Figs. 33 and 34 for $\epsilon=0$. The difference between the two will be attributed to the sign of Γ in (3.3). When Γ is positive, as in the case of $\epsilon=1$, the renormalized output $Y(z)$ takes the form as shown in Fig. 12(b) or 13(b), and hence there appears a region of z in which $|h|=\theta$, implying the occurrence of the δ function in the local field distribution (4.32). As was mentioned previously, even when the narrowing limit of the width of the local field distribution with $\epsilon=1$ is attained for $\alpha \leq \alpha_0$, the distribution of the scaled output $\tilde{P}(V)$ exhibits, besides a finite measure at $V=0$ and 1, a component which is distributed all the way from $V=0$ to 1. Results of numerical simulations indeed confirm the appearance of the continuous component of the $\tilde{P}(V)$, an example of which is given in Fig. 39. This is also in good agreement with the result of the SCSNA shown in Fig. 27.

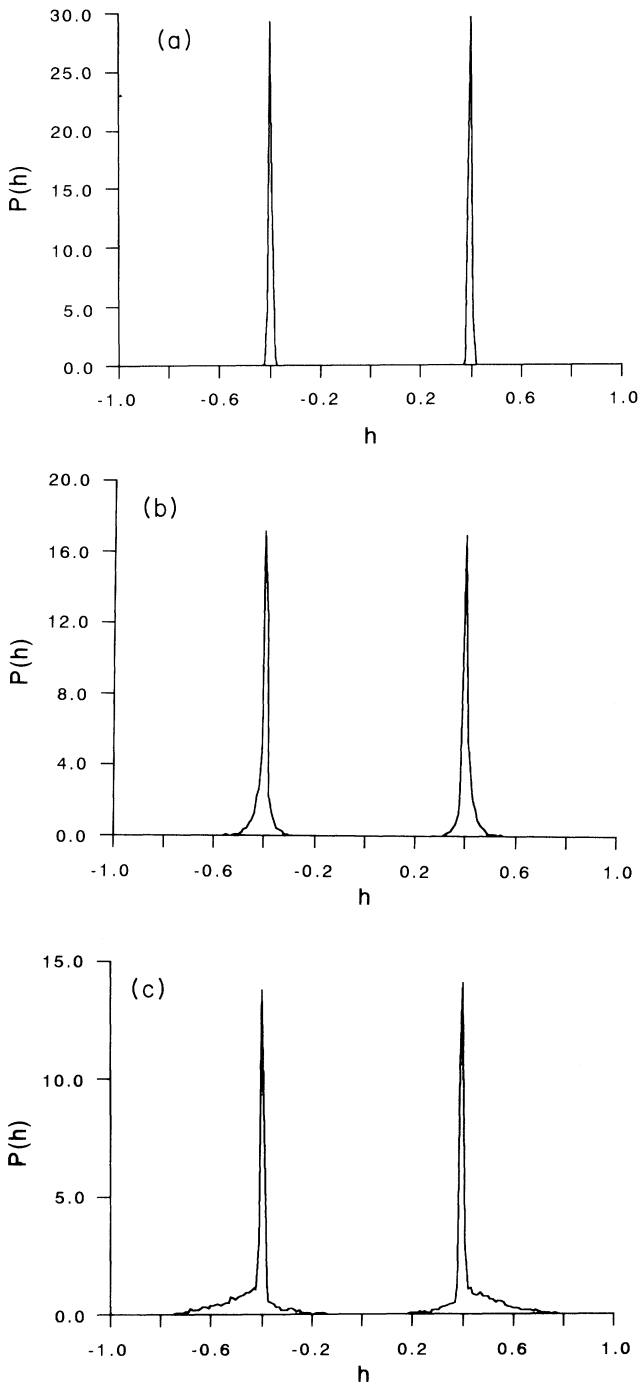

FIG. 38. Local field distribution $P(h)$ in the retrieval state ($\epsilon=1$) with $\theta=0.4$ obtained from numerical simulations ($N=200$) for (a) $\alpha=0.25$, (b) $\alpha=0.5$, (c) $\alpha=0.75$.

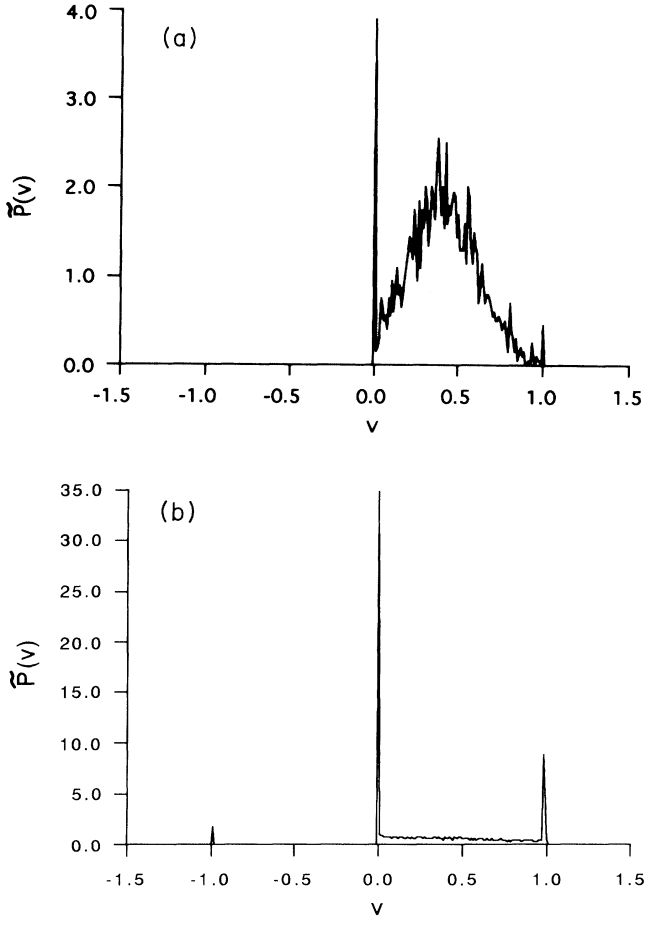

FIG. 39. Output distribution $\tilde{P}(V)$ in the retrieval state ($\epsilon=1$) under the same condition as Fig. 38: (a) $\alpha=0.25$, (b) $\alpha=0.75$. In the simulations the transfer function with $\delta=0.005$ is used together with the dynamics (2.1b) ($I=0$).

V. SUMMARY AND DISCUSSIONS

We have presented a reformulated scheme of the self-consistent signal-to-noise analysis (SCSNA), which elucidates the self-consistent treatment of the local fields of neurons, i.e., renormalization of the naive noise in obtaining the set of order-parameter equations for retrieval states. Using the SCSNA, we have explored properties of neural networks for the qualitatively different two types of transfer functions F^{M} (center-cutoff-type) and F^{NM} (end-cutoff-type), which are derived by cutting off the activity of a neuron with binary output to formally describe a three-state neuron taking output values on -1, 0, and 1. The SCSNA has proved powerful in exploring microscopic as well as macroscopic properties of the analog neural networks. The main results of equilibrium properties of the networks are concerned with the enhancement of the storage capacity and the phase-transition-related issues brought about by the choice of those transfer functions and the introduction of the self-couplings. Our conclusions drawn from the theoretical results together with the results of numerical simulations are summarized as follows.

Concerning the SCSNA applied to the analog neural networks, we note the following.

(1) So far as the retrieval states given as stable fixed points of the updating equations of the analog neural networks are concerned, the SCSNA yields a detailed description of the mechanism of determining the local field distribution of neurons, which plays an important role in obtaining the retrieval phase boundary.

(2) The local field distribution of the analog neural networks, in general, is non-Gaussian due to the presence of the output proportional term ΓY in the local field which arises from the renormalization of the so-called naive noise.

(3) The SCSNA is capable of dealing with the occurrence of the new type of phase transition as has been found for transfer functions F^{NM}.

(4) The Maxwell rule used in applying the SCSNA has proved not only to be valid even for nonsigmoidal-type transfer functions, but also to play a crucial role for the occurrence of the new type of phase transition.

Regarding the network properties investigated, in the case of the center-cutoff-type transfer function F^{M}, we note the following.

(1) The spin-glass state emerges from the paramagnetic state through a first-order phase transition in the phase diagram of α and θ, and there exists a certain small region of the retrieval phase in which the spin-glass state is not allowed to coexist. This implies the reduction of the number of spurious states associated with spin-glass states.

(2) The behavior of the storage capacity with changing θ is qualitatively the same as that of the analog networks of a sigmoidal transfer function with changing analog gain: θ can be viewed as playing the role of the analog gain.

(3) The effect of the self-couplings is to increase the storage capacity within the maximum value of 0.138.

In the case of the end-cutoff-type transfer function F^{NM}, we note the following.

(1) The networks exhibit a large enhancement of the storage capacity α_c such that with decreasing θ from $\theta=\infty$, α_c increases up to a maximum of ≈ 0.42 ($\theta \cong 0.7$) and afterwards decreases to vanish at $\theta=0$.

(2) While the $\alpha_c(\theta)$ with $\theta \gtrsim 1$ can be determined by the SCSNA as the upper bound of α ensuring the existence of the retrieval solutions, the one with $\theta \lesssim 1$ is given as the value of α exhibiting the onset of instability of the retrieval solution of the SCSNA.

(3) The shape of the non-Gaussian distribution of the local field depends crucially on the sign of Γ.

(4) When $\theta < 1$, the networks undergo a kind of phase transition at $\alpha=\alpha_0(\theta)$, which arises from the disappearance of the standard type of retrieval states with $r \neq 0$, as the loading rate α is decreased from α_c. Below the phase-transition point, the width of the local field distribution $\sqrt{\alpha r}$ vanishes and hence memory retrieval without errors ($g=1$) is achieved.

(5) The effect of the self-couplings on the enhancement of the storage capacity is conspicuous for small values of θ; the self-couplings increase the stability of the retrieval solutions claimed by the SCSNA to suppress the oscillatory instability present in the case of $\epsilon=0$. A part from the problem of the appearance of spurious states, an optimum value of ϵ exists for each θ to maximize the storage capacity.

(6) The self-couplings also modify the behavior of the networks which is related to the occurrence of the new type of phase transition, giving rise to an increase in the critical loading rate α_0 for $\epsilon \leq 1$. When $\epsilon > 1$, the phase transition disappears.

The occurrence of the new type of phase transition due to the vanishing of noise in the local fields implies that perfect (errorless) memory retrieval is ensured even with an extensive number of stored patterns under the local learning rule of the Hebb type [34]. The phenomenon will be generic for a certain class of transfer functions giving rise to the occurrence of jumps in the renormalized output function Y which results from the use of the Maxwell rule as in the case of $\epsilon < 1$ with F in (4.1) and $F_{0^+\delta}$ in Fig. 9. Even in the case of the transfer function $F_{0^+\delta}$ with a small δ (>0), which destroys the errorless memory retrieval states to bring about the $r \neq 0$ phase for α up to 2δ (i.e., $0 < \alpha < 2\delta$), the $r=0^+$ phase still remains to exist for the interval $2\delta < \alpha < \alpha_0(\theta)$, as long as δ satisfies $2\delta < \alpha_0(\theta)$.

It is of interest to notice that the occurrence of the transition with respect to noise in the local field is affected considerably by the self-couplings and that indeed for $\epsilon > 1$ the transition disappears. The present study has revealed that in the case of $\epsilon=1$ with the transfer function (4.1), the $r=0^+$ phase below the transition point can be described by a certain limit of the solution of the order-parameter equations of the SCSNA. The $r=0^+$ phase for $\epsilon < 1$, on the other hand, can only be partially understood based on the SCSNA (4.10); whereas its property is well described by (4.10a) and (4.10b) alone, the third equation (4.10c) remains inconsistent with those two equations in the limit $r \to 0$ and $U \to -\infty$. Exploring the probabilistic structure of the $r=0^+$ phase as well as

searching for a necessary and sufficient condition for the existence of the transition are now under way.

An attempt to obtain a remarkable enhancement of the storage capacity in Hopfield-type neural networks was made previously based on networks with sparsely encoded patterns [13,31,32]. The large enhancement of the storage capacity found in the present study of the end-cutoff-type transfer functions can be attributed to the nonmonotonicity of the transfer function and hence of the renormalized output $Y(z)$. Recently, Morita, Yoshizawa, and Nakano [33(a)] and Morita [33(b)] suggested use of nonmonotonic neurons to make such improvements of the network performances as reduction of the spurious states and enhancement of the storage capacity. Using the systematic method of the SCSNA with the nonmonotonic transfer functions of the end-cutoff-type, we have obtained the results which are consistent with their suggestion from numerical simulations. The present work has paved the way to a systematic analysis leading to a quantitative as well as qualitative understanding of the mechanism of the enhancement of the storage capacity in the networks of nonmonotonic neurons. In fact, taking advantage of the SCSNA which is available for a wide class of transfer functions ensuring fixed-point-type attractors for the updating dynamics (2.1), we can show that in general a similar enhancement of the storage capacity occurs in networks having nonmonotonic transfer functions. Details of the study will be reported elsewhere.

Finally we will comment on an attempt to exploit the self-couplings aiming at the enhancement of the storage capacity. Worth noting is the qualitative difference in the effect of the self-couplings between the two types of transfer functions, F^{M} and F^{NM}. The effect of the self-couplings has turned out not to be of uniformity but to depend substantially on the qualitative difference of the transfer functions. One may consider that dealing with the self-couplings does not make sense in physiological nervous systems since a single neuron is not likely to extend a self-coupling to itself. However, it may be possible that local clusters of neurons serve as functional units in the information processing of those systems and thereby local connections within the clusters give rise to feedback loops representing effective self-couplings. In this case, overall input-output relations of the clusters of neurons will also possibly be represented by effective transfer functions which can take a variety of shapes including the one with nonmonotonicity. In artificial intelligence engineering, on the other hand, it will be easy to implement the self-couplings on artificial neural network circuitries with rather arbitrary transfer functions in order to achieve the enhancement of the storage capacity. The present work has revealed that a combination of the introduction of a certain amount of self-couplings and the use of appropriately chosen transfer functions gives rise to a promising expectation of a considerable enhancement of the storage capacity. Since a large amount of the self-couplings deteriorates the network performance due to an increase in the number of spurious states, a further study will be required to evaluate the total effect of the self-couplings on the network performances.

ACKNOWLEDGMENTS

This work is partially supported by the Grant-in-Aid for Scientific Research (Grant No. 02640289) and the Grant-in-Aid for Encouragement of Young Scientist (Grant No. 03740205) from the Ministry of Education.

APPENDIX A: DERIVATION OF THE AGS RESULT USING THE SCSNA

For the sake of simplicity we assume $a=0$ for the stored patterns. It was shown by means of the cavity method in the spin-glass theory that equilibrium states of the Ising spin neural networks of AGS with temperature $1/\beta$ can be equivalently described by the so-called TAP equation with the Onsager reaction field term, which should read [15]

$$S_i=\tanh\left[\beta\left[\sum_{j=1}^{N}J_{ij}S_j-\frac{\alpha S_i}{1-\beta(1-q)}\right]\right], \tag{A1}$$

with

$$q=\frac{1}{N}\sum_{j=1}^{N}S_j^2 . \tag{A2}$$

The self-coupling related term of the local field of the TAP equation (A1) is seen to just arise from the Onsager reaction field

$$h_{\mathrm{ORF}}=-\frac{\alpha S_i}{1-\beta(1-q)} .$$

For the purpose of recovering the AGS result, it will suffice to show $\Gamma=0$. When applying the SCSNA to (A1), one obtains ΓY, the output proportional term in the local field, as the sum of the squeezed output γY [see (2.19)] and the Onsager reaction field h_{ORF}. Then it follows that

$$\Gamma=\frac{\alpha}{K}-\frac{\alpha}{1-\beta(1-q)} . \tag{A3}$$

The renormalized output (2.28) is

$$Y(\xi^{(1)},\bar{z})=\tanh\{\beta[\xi^{(1)}m^{(1)}+I+\bar{z}+\Gamma Y(\xi^{(1)},\bar{z})]\} . \tag{A4}$$

Since differentiation of (A4) with respect to $\bar{z}$ yields

$$\frac{dY}{d\bar{z}}=\beta\{\mathrm{sech}^2[\beta(\xi^{(1)}m^{(1)}+I+\bar{z}+\Gamma Y)]\}\left\{1+\Gamma\frac{dY}{d\bar{z}}\right\}, \tag{A5}$$

one has from (2.24) and (A2)

$$\begin{aligned}1-K&=\left\langle\!\left\langle\frac{d}{d\bar{z}}Y(\bar{z})\right\rangle\!\right\rangle\\&=\beta(1-q)\\&\quad+\Gamma\left\langle\!\left\langle\beta\frac{dY}{d\bar{z}}\mathrm{sech}^2[\beta(\xi^{(1)}m^{(1)}+I+\bar{z}+\Gamma Y)]\right\rangle\!\right\rangle .\end{aligned} \tag{A6}$$

Substitution of (A3) yields

$$\Gamma X=0 , \tag{A7}$$

with

$$X=\left\langle\!\left\langle \beta\frac{dY}{d\bar{z}}\mathrm{sech}^2[\beta(\xi^{(1)}m^{(1)}+I+\bar{z}+\Gamma Y)]\right\rangle\!\right\rangle - \frac{K[1-\beta(1-q)]}{\alpha} . \tag{A8}$$

Assuming $X\neq 0$, one obtains $\Gamma=0$.

APPENDIX B: DERIVATION OF THE SET OF EQUATIONS DESCRIBING THE $r=0^+$ PHASE WITH $\epsilon=1$ AS WELL AS (4.29)

We present a systematic derivation of (4.29) on the basis of the SCSNA order-parameter equations (2.30) and show that the retrieval phase below the transition point α_0 (i.e., $r=0^+$ phase) can be properly described by taking the limit $r\to 0+$ of the SCSNA equations in the case of $\epsilon=1$.

Suppose the transfer function F to be given by the $F_{0^+\delta}$. The renormalized output $Y(z)$ in the case of $0<\Gamma<\theta$ then is readily solved as

$$Y(z)=\begin{cases} 0, & z<z_1,\ z_4<z \\ \dfrac{-(\theta+\delta)-m-\sqrt{\alpha r}z}{\Gamma+2\delta}, & z_1<z<z_2 \\ \dfrac{\theta+\delta-m-\sqrt{\alpha r}z}{\Gamma+2\delta}, & z_3<z<z_4 \\ -1, & z_2<z<z_0 \\ 1, & z_0<z<z_3 , \end{cases} \tag{B1a}$$

with

$$\begin{aligned} z_0&=\frac{-m}{\sqrt{\alpha r}} , \\ z_1&=\frac{-(\theta+\delta)-m}{\sqrt{\alpha r}} , \\ z_2&=\frac{-(\theta-\delta)+\Gamma-m}{\sqrt{\alpha r}} , \\ z_3&=\frac{\theta-\delta-\Gamma-m}{\sqrt{\alpha r}} , \\ z_4&=\frac{\theta+\delta-m}{\sqrt{\alpha r}} . \end{aligned} \tag{B1b}$$

The SCSNA order-parameter equations (2.30) for the $Y(z)$ take the form

$$m=\frac{-(\theta+\delta)-m}{\Gamma+2\delta}N[z_1,z_2]-N[z_2,z_0]+N[z_0,z_3]+\frac{\theta+\delta-m}{\Gamma+2\delta}N[z_3,z_4] + \frac{\sqrt{\alpha r}}{(\Gamma+2\delta)\sqrt{2\pi}}(e^{-z_2^2/2}+e^{-z_4^2/2}-e^{-z_1^2/2}-e^{-z_3^2/2}) , \tag{B2a}$$

$$(1-U)^2 r=N[z_2,z_0]+N[z_0,z_3]+\frac{\alpha r+(\theta+\delta+m)^2}{(\Gamma+2\delta)^2}N[z_1,z_2]+\frac{\alpha r+(\theta+\delta-m)^2}{(\Gamma+2\delta)^2}N[z_3,z_4] + \frac{\alpha r}{(\Gamma+2\delta)^2\sqrt{2\pi}}(z_1e^{-z_1^2/2}+z_3e^{-z_3^2/2}-z_2e^{-z_2^2/2}-z_4e^{-z_4^2/2}) - \frac{2\sqrt{\alpha r}(\theta+\delta+m)}{(\Gamma+2\delta)^2\sqrt{2\pi}}(e^{-z_2^2/2}-e^{-z_1^2/2})+\frac{2\sqrt{\alpha r}(\theta+\delta-m)}{(\Gamma+2\delta)^2\sqrt{2\pi}}(e^{-z_4^2/2}-e^{-z_3^2/2}) , \tag{B2b}$$

$$U\sqrt{\alpha r}=-\frac{\sqrt{\alpha r}}{\Gamma+2\delta}(N[z_1,z_2]+N[z_3,z_4])+\frac{2}{\sqrt{2\pi}}e^{-z_0^2/2} . \tag{B2c}$$

We consider taking the limit $\delta\to+0$ of the above set of equations. Then, it is expected that $r\to+0$, when $\alpha\leq\alpha_0$. Following the same line of reasoning as in deriving (4.26), we assume

$$\lim_{\delta\to 0}(\theta+\delta-m)=0 , \tag{B3a}$$

$$\lim_{\delta\to 0}z_4=\hat{z_4} , \tag{B3b}$$

$$\lim_{\delta\to 0}(z_4-z_3)=\lim_{\delta\to 0}\frac{2\delta+\Gamma}{\sqrt{\alpha r}}=\hat{w} , \tag{B3c}$$

together with

$$\lim_{\delta\to 0}\frac{2\delta}{\sqrt{\alpha r}}=\lambda . \tag{B3d}$$

Noting $(1-U)^2r=\alpha^2 r/\Gamma^2$ and taking the limit $\delta\to+0$ of (B2) with use of the above relations, one obtains the set of equations for $\hat{z}_4,\hat{w}$, and λ:

$$\theta=N[-\infty,\hat{z_4}-\hat{w}]+\frac{\hat{z_4}}{\hat{w}}N[\hat{z_4}-\hat{w},\hat{z_4}] + \frac{1}{\hat{w}\sqrt{2\pi}}(e^{-\hat{z}_4^2/2}-e^{-(\hat{z}_4-\hat{w})^2/2}) , \tag{B4a}$$

$$\frac{\alpha}{(\hat{w}-\lambda)^2}=N[-\infty,\hat{z_4}-\hat{w}]+\frac{1+\hat{z}_4^2}{\hat{w}^2}N[\hat{z_4}-\hat{w},\hat{z_4}]$$
$$+\frac{1}{\hat{w}^2\sqrt{2\pi}}[(\hat{z}_4-\hat{w})e^{-(\hat{z}_4-\hat{w})^2/2}-\hat{z}_4e^{-\hat{z}_4^2/2}]$$
$$+\frac{2\hat{z}_4}{\hat{w}^2\sqrt{2\pi}}(e^{-\hat{z}_4^2/2}-e^{-(\hat{z}_4-\hat{w})^2/2}) , \quad \text{(B4b)}$$

$$\frac{-\alpha}{\hat{w}-\lambda}=-\frac{1}{\hat{w}}N[\hat{z_4}-\hat{w},\hat{z_4}] . \quad \text{(B4c)}$$

We see that combining (B4b) and (B4c) together with rewriting $\hat{z_4}$ and $\hat{w}$ as z_4 and w yields (4.29). Equations (B4) describe the retrieval state without errors (i.e., $r=0^+$) for $\alpha\leq\alpha_0$. In other words, the spin-glass order parameter

$$q=\frac{\alpha}{(\hat{w}-\lambda)^2} , \quad \text{(B5)}$$

and the renormalized output $Y(z)$ can be determined from the solution of (B4). As is described in text, (B4) yields its solution only for $\alpha\leq\alpha_0$.

[1] J. J. Hopfield, (a) Proc. Natl. Acad. Sci. USA **79**, 2554 (1982); (b) **81**, 3088 (1984); (c) J. J. Hopfield and D. W. Tank, Biol. Cybern. **52**, 141 (1985).

[2] S. Grossberg, Neural Networks **1**, 17 (1988); R. J. MacGregor, *Neural and Brain Modelling* (Academic, New York, 1987).

[3] D. J. Amit, *Modelling Brain Function* (Cambridge University Press, Cambridge, England, 1989).

[4] T. Geszti, *Physical Models of Neural Networks* (World Scientific, Singapore, 1990).

[5] *Models of Neural Networks,* edited by E. Domany, J. L. van Hemmen, and K. Schulten (Springer, New York, 1991).

[6] E. Gardner, J. Phys. A **19**, L1047 (1986).

[7] D. J. Amit, H. Gutfreund, and H. Sompolinsky, Phys. Rev. Lett. **55**, 1530 (1985); Ann. Phys. (N.Y.) **173**, 30 (1987).

[8] M. Shiino and T. Fukai, J. Phys. A **23**, L1009 (1990).

[9] T. Fukai and M. Shiino, Phys. Rev. A **42**, 7459 (1990).

[10] T. Fukai and M. Shiino, J. Phys. A **25**, 2873 (1992).

[11] R. Kühn, S. Bös, and J. L. van Hemmen, Phys. Rev. A **43**, 2084 (1991); R. Kuhn, in *Statistical Mechanics of Neural Networks,* edited by L. Garrido, Springer Lecture Notes in Physics Vol. 398 (Springer-Verlag, Heidelberg, 1990).

[12] C. M. Marcus, F. R. Waugh, and R. M. Westervelt, Phys. Rev. A **41**, 3355 (1990); F. R. Waugh, C. M. Marcus, and R. M. Westervelt, *ibid.* **43**, 3131 (1991).

[13] A. Treves, Phys. Rev. A **42**, 2418 (1990).

[14] D. J. Thouless, P. W. Anderson, and R. G. Palmer, Philos. Mag. **35**, 593 (1977).

[15] M. Mezard, G. Parisi, and M. A. Virasoro, *Spin Glass Theory and Beyond* (World Scientific, Singapore, 1987).

[16] M. Shiino and T. Fukai, J. Phys. A **25**, L375 (1992).

[17] G. Weisbuch and F. Fogelmann-Soulie, J. Phys. (Paris) Lett. **46**, L623 (1985).

[18] R. J. McEliece, E. C. Posner, E. R. Rodemich, and S. S. Venkatesh, IEEE Trans. Inf. Theory **IT-33**, 461 (1987).

[19] S. Amari and K. Maginu, Neural Networks **1**, 63 (1988).

[20] P. Peretto, J. Phys. (Paris) **49**, 711 (1988).

[21] E. Domany, W. Kinzel, and R. Meir, J. Phys. **22**, 2081 (1989).

[22] T. Fukai and M. Shiino, J. Phys. A **25**, 4799 (1992).

[23] H. Rieger, J. Phys. A **23**, L1273 (1990).

[24] J. L. van Hemmen, Phys. Rev. Lett. **49**, 409 (1982).

[25] U. Riedel, R. Kuhn, and J. L. van Hemmen, Phys. Rev. A **38**, 1105 (1988).

[26] A. C. C. Coolen and Th. W. Ruijgrok, Phys. Rev. A **38**, 4253 (1988).

[27] M. Shiino, H. Nishimori, and M. Ono, J. Phys. Soc. Jpn. **58**, 763 (1989).

[28] M. Shiino, J. Stat. Phys. **59**, 1051 (1990).

[29] T. Fukai and M. Shiino, Phys. Rev. Lett. **64**, 1465 (1990).

[30] H. Nishimori, T. Nakamura, and M. Shiino, Phys. Rev. A **41**, 3346 (1990).

[31] C. J. Perez Vicente and D. J. Amit, J. Phys. A **22**, 559 (1989).

[32] S. Amari, Neural Networks **2**, 451 (1989).

[33] (a) M. Morita, S. Yoshizawa, and K. Nakano, Trans. Inst. Electron. Info. Commun. Eng. **J73-DII**, 232 (1990) (in Japanese); (b) M. Morita, Neural Networks **6**, 115 (1993).

[34] M. Shiino and T. Fukai, J. Phys. A (to be published).